Creation and Detection of Vector Bessel Beams

University of Fort Hare
Together in Excellence

Idisi David Omoefe

Student number: 201505651

A thesis submitted to the University of Fort Hare,

Faculty of Science and Agriculture in fulfillment of the

requirement for the Degree of Masters of Science in Physics

Supervisors:

Professor Golden Makaka

Professor Andrew Forbes

2016

Abstract

Bessel beams are optical fields which falls into the category of non-diffracting beams. Vector Bessel beams are vector beams possessing cylindrical symmetry. Cylindrically symmetric beams tend to have a tight focal point during propagation. The tight focal beam nature of vector Bessel beams makes them a good potential in various facets of science such as biological optical trapping, wireless communications, remote sensing, microscopy etc. In this research work, vector Bessel beams were generated using the phase of an Axicon that was encoded into a spatial light modulator. Firstly, scalar Bessel beams which possess linear polarization were generated and converted to circularly polarized vector beams by the use of a q-plate. The orbital angular momentum (OAM) modes that are embedded in the vortex beams were detected using modal decomposition technique. This was implemented for both the scalar and vector case using a quarter wave plate. The measure of the degree of non-separability of the vector Bessel beams using tomographic quantum tools was also implemented where the density matrix was reconstructed. The concurrence and fidelity which explore the measure of vectorness of both scalar and vector Bessel beams were calculated from the density matrix. The obtained results show that the spatial modes and polarization are coupled in the vector case as expected.

Acknowledgments

I would like to express my profound gratitude to:

- My host supervisor, Professor Golden Makaka for the opportunity given to me to do my research thesis in Photonics, Financial support for the experimental work at structured light laboratory, Johannesburg and also the pain staking review of the research work.
- My supervisor, Professor Andrew Forbes for the contribution towards the concept of the research work, expert direction and creating an enabling environment at the structured light laboratory.
- The entire team at the structured light laboratory. they made my entire stay very accomodating and conducive
- Photonics initiative of South Africa (PISA) for funding photonics research at department of Physics, University of Fort Hare.
- South African National research foundation (NRF) for financial support towards my masters program (grant number 100129).
- Ndagano Bievenu at the structured light laboratory for all the insight into the experimental work. Thanks for your time and expert opinion.
- My parents Mr and Mrs M. O Oruegwo for the encouragement when things were very difficult and discouraging me from quitting.

God bless you all.

This research thesis is dedicated to my late wife Mrs Idisi Enoh, it is painful that you are no longer here with us to see what you persevered for.

Candidate's Declaration

I declare that this thesis is my own, unaided work. It is being submitted for the degree of Masters of Science in the University of Fort Hare, Alice. It has not been submitted before for any degree or examination at any other University.

____

Idisi David Omoefe

________________ day of ________________ 2016

Summary

Non-diffracting vector Bessel beams are vector beams possessing cylindrical symmetry. Cylindrical symmetric beams tend to have a tight focal point during propagation. The tight focal beam nature of Bessel beams makes them a potential resource in various avenues of science ranging from optical tweezing to microscopy. Vector beams have also proved to be useful in optical communication. Information can be encoded in the orbital angular momentum (OAM) of the beam and thus can be used to transport information across reasonable distances without diffracting.

The goal of this project is to generate and detect vector Bessel beams using digital Axicons. In chapter one, a brief overview of Bessel beams is presented. This is followed by problem statement, aims, objective, materials and methods that is intended for the research work.

In chapter two, the characteristics of Bessel beams is presented, this is followed by an overview of orbital angular momentum, vector fields and their polarization. This is followed by a brief review of cylindrical vector beams and their mathematical implications.

A review of spatial light modulators (SLMs) and how they can be used in the generation of Bessel beams alongside Axicons and annular slits is presented in chapter three. Experimental work regarding the generation of scalar Bessel beams using the phase of an Axicons encoded into an SLM is presented. The OAM constituent of the scalar Bessel beams was detected using the technique of modal decomposition.

In chapter four, q-plate and its working principle is presented. The experimental work involving the generation of vector Bessel beams using the aforementioned birefringent material otherwise called a q-plate is presented. The q-plate introduced OAM into the light beam and the OAM components of the vector beam was detected using modal decomposition. A quarter waveplate was used to decompose the vector beam into two linearly polarized scalar beams and modal decomposition was independently performed on the scalar beams. The results obtained was in correlation with literature.

The vectorness which involves the measure of the non-separability of the spatial mode and polarization state of vector beams was also measured using quantum tomography tool. Vectorness of the vector beams can be visualized as entanglement of quantum states. A density matrix was reconstructed from the quantum tomography measurement. The concurrence C which is the measure of the degree of entanglement was calculated from the density matrix. Depending on the coupling of the entangled state, the concurrence ranges from 0 to 1. The states are unentangled (scalar beams) if the the value of concurrence approaches 0. Fidelity F which is the measure of the closeness of the non-separability of the spatial mode and polarization was also calculated from the density matrix. Both values were found to be $C = 0.76 \pm 0.01$ and $F = 0.86 \pm 0.01$ respectively. In the scalar case, the values obtaind are $C = 0.05 \pm 0.01$ and $F = 0.06 \pm 0.01$ respectively. These values are in good agreement with literature as expected.

Contents

List of Figures

Chapter 1

Introduction

The theory of rectilinear propagation of light stipulates that light travels along a straight path, however, it diffracts when it encounters an obstacle during propagation [Stamnes, (1986)]. Bessel beams are non-diffracting light fields with beams of infinite rings covering an infinite propagation distance with infinite amount of energy (in terms of the beams wavelength with the centre of the beam having a diameter of about three-quarters of the wavelength). Bessel beams (BBs) are not affected by a transverse spread after undergoing a long distance of propagation along a plane with relevant energy density and well defined intensity distributions [Durnin et al., (1987)]. The Bessel beam amplitude is described by the Bessel function and Bessel beams are generally solutions to the Helmholtz wave equation [Griffiths and Reed, (1999)] given as:

$$(\nabla^2 + k^2)E(x, y, z) = 0 \tag{1.1}$$

where $k = 2\pi/\lambda$ is the wave number. Bessel beams are used in many applications such as in optical tweezing [Arlt et al, 2001], precision drilling [Kohno, M. and Matsuoka, Y., 2004] and transferring of encoded data [Garcés-Chávez, V. et al, (2003)]. The data carrying capacity of Bessel beam is a function of its property to retain its shape after long distance of propagation. Bessel Beams are beams whose electric field can be described by

$$E(r, \varphi, z) = E_0 \exp(ik_z z) J_0(k_r r) \tag{1.2}$$

where E_0 is the amplitude of the optical wave, k_r is the radial wave vector which depicts the spacing between the rings, k_z is the longitudinal wave vectors, r is the transverse coordinate and z represents the direction of propagation, $J_0(k_r r)$ is the zeroth-order Bessel function of the first kind describing the behaviour of the optical field [Duocastella and Arnold, (2012)].

1.1 Problems statement

Vector Bessel beams can be described as having a coupling of spatial modes with inhomogenous state of polarization. They propagate better through atmospheric turbulence due to temperature fluctuation and this makes them very useful for wireless optical communication and remote sensing and they also produces tight focusing which are very useful for micro-particle manipulation [Arlt et al, 2001, Kohno, M. and Matsuoka, Y., 2004]. Generating Bessel beams experimentally can be rather difficult due to the infinite energy requirement. The energy in the beam is expected to propagate to infinity hence requiring an infinite energy source. An experimental setup for the generation of Bessel beams that satisfies the energy and propagation distance requirement is highly unlikely [Arlt, J., and K. Dholakia, (2000)]. In most cases, a quasi-Bessel beam is used. This is like an approximation of a Bessel beam which has the behaviour of BBs but with finite distance.

Various methods for generating Bessel beams has been explored previously [Litvin et al., (2015), **?**, McGloin and Dholakia, (2005)]. Recent research on Bessel beam generation involved physical Axicons and these Axicons are difficult to align. However, in the case of a digital Axicons, it is much easier to implement experimentally. Where other researchers used the digital method, emphasis was not given to vector Bessel beams rather scalar beams. Furthermore, where vector Bessel-beams [Dudley et al., (2013)] were generated, digital Axicons were not used but rather digital annular slits were utilized. Although digital annular slits and Axicons yields the same result, digital Axicons proves more convenient. In all these cases, the measure of vectorness were not considered. In this research work, the following questions were answered.

- What is the proposed method for the vector beam generation?
- How will the beams be detected?
- How will the vectorness of the vector Bessel beams be measured?

1.2 Aims and Objectives

This project was aimed at exploring novel ways to generate, detect and test vector Bessel beams. To achieve this aim, the following objectives were set:

- To generate Bessel beams using both geometric and dynamic phase of light.
- To generate vector Bessel beams using a q-plates which is a birefringent optical device.
- To detect Bessel beams by analysis of their amplitude and phase.
- To use quantum tomography tools to test the vectorness of these beams.

1.3 Materials and Methods

Different optical elements such as mirrors, lenses, spatial light modulators amongst others were used. The experimental procedures includes:

- Generation of Bessel beams using optical elements.
- Detection of the orbital angular momentum modes using modal decomposition technique.
- Measurement of the degree of non-seperability of the vector beams using quantum tomography tools.

1.4 Structure of the dissertation

The structure of the research is such that; in chapter one, Bessel beams are introduced with emphasis on the aims and objective with materials and method of the research work, chapter two deals with the characteristics of Bessel beams with emphasis on vector fields and polarization of the vector fields. Chapter three focuses on the overview of scalar Bessel beams as well as the method of generation and detection. Experimental procedures and results are also presented in this section. Chapter four covers the generation and detection of vector Bessel beams alongside the measure of vectorness of the Bessel beams (both scalar and vector cases). Chapter five gives the conclusion of the entire research as well as future work.

1.5 Summary

Bessel beams are nondiffracting optical fields which are solutions to Maxwell Helmoltz equation. A brief overview of vector Bessel beams was presented with the current trend in the generation techniques of Bessel beams. Problem statement, aims and objectives as well as the methodology that was explored in the research work were briefly presented.

Chapter 2

Bessel beams and their characteristics

2.1 Introduction

Bessel beams are categorized into the family of non-diffracting beams with infinite number of rings propagating over an infinite region with an infinite amount of energy. Bessel beams are characterized by beam robustness, phase dislocation, beam energy e.t.c [**?**].

2.2 Characteristics of Bessel Beams

Bessel beams exhibit some features that makes them unique as compared with other beams such as Gaussian, Hermite-Gaussian and Laguerre-Gaussian beams. Some of these characteristics are given below :

Beam robustness is the resistance of BBs to amplitude and phase distortions. The transverse intensity profile is usually not interfered by non-transparent obstacle that is generated during propagation through free space and is referred to as self healing effect. This self-healing effect results in the restoration of the beam initial transverse intensity profile after certain distance behind the distorting obstacle. Figure 2.1 illustrates how the self-healing process of Bessel beams evolves.

Figure 2.1 shows how some of the incident light is blocked by the obstacle during

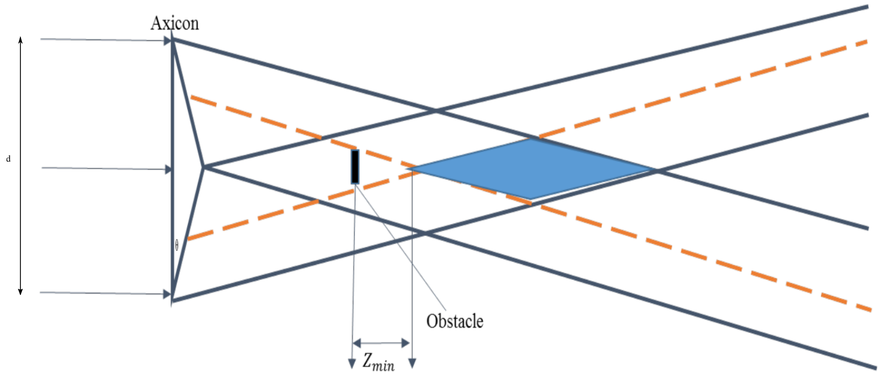

Figure 2.1: Illustration of the reconstruction of BBs after encountering an obstable, the diamond-shaped region after the obstacle represents the reconstructed Bessel beams. z_{min} is the minimum distance after which the beams starts reconstructing, d is the diameter of the input beam and θ is the Axicon opening angle. The optical field after the Axicon are in the form of conical waves and they propagate around the obstacle and reconstructs a Bessel beam profile [Bouchal, 2003].

propagation. The distortion created by the obstacle leads to a shadow region z_{min} (minimum distance after which the BB starts reconstructing after the obstacle). The shadow region occurs till the light beams reconstructs. The minimum length of the shadow region is given by :

$$z_{min} = \frac{d}{2\tan\theta} \tag{2.1}$$

where the parameters d is the diameter of the obstacle which is enough to block the centre of the propagating beam and θ is the axicon angle [Arlt, J., and K. Dholakia, (2000)].

Beam Energy is the power of the beam which is circulated around the rings of the BBs. The energetic property of BBs can be ascribed to the Poynting vector P. The Poynting vector indicates the energy flux density in terms of energy transfer. The Poynting vector is given as:

$$\hat{P} = E \times H \tag{2.2}$$

where E and H are the electric field and magnetic field vector respectively. The Poynting vector can be decomposed into transverse (P_T) and longitudinal (P_L) components and is given as:

$$\hat{P} = P_T + P_L \tag{2.3}$$

The transverse component can be further decomposed into

$$P_T = P_l + P_\varphi \tag{2.4}$$

where P_l is the radial component and P_φ being the azimuthal component. If $P_l = 0$, the electromagnetic energy can flow in the azimuthal direction [Bouchal et al., (1998)].

Phase dislocation is the phase singularity of light beams. By singularity, it implies that the beam has an imperfection in its wavefront i.e a screw-type defect. The amplitude of the beam at that particular phase is zero thereby producing an optical vortex. It is expected that the amplitude of the optical field tends to zero. The zero amplitude yield a zero complex and imaginary component and an infinite phase defect [Basistiy et al., (1995)]. This vortex behaviour is usually termed wavefront dislocation. BBs tend to have phase dislocation, the complex amplitude of the field is given as:

$$U(x, y) = J_n(x, y) \exp\left[in \arctan\left(\frac{y}{x}\right) - k_z z\right] \tag{2.5}$$

where $J_n(x, y)$ is the Bessel function of the order n with $n \subset \mathcal{Z}$. $\arctan\left(\frac{y}{x}\right)$ and k_z are the topological quantum number and propagation constant respectively [Schwarz et al., (2002), Bouchal et al., (1998)]. The wave front dislocation can be easily measured using an interferometer [Berkhout G. and Marco W., (2010)].

Free-wave mode decomposition is the decomposition of light beams into plane waves. BBs exhibit a special mode in cylindrical coordinate such that it decomposes into other cylindrically symmetric wave fields. Consider a spherical wave given as:

$$\frac{e^{iwR/v}}{R} = \frac{1}{2\pi}\int_{\infty}^{\infty} dk_1 dk_2 \frac{1}{k_3} e^{i(k_1x_1+k_2x_2+k_3|x_3|)} \tag{2.6}$$

Where $k_3 = (w^2/v^2 - k_1^2 - k_2^2)^{1/2}$ with $ik_3 > 0$ and $k_3 > 0$. A spherical wave can also take the form:

$$\frac{e^{iwR/v}}{R} = i\int_{0}^{\infty} dk_r \frac{k_r}{k_3} J_0(k_r r) e^{ik_3|x_3|} \tag{2.7}$$

Where $k_r^2 = k_1^2 + k_2^2$ is the wave number, J_0 can be written in terms of the Hankel first and second kind given as:

$$J_0 = \frac{1}{2}(H_0^{(1)} + H_0^{(2)}) \tag{2.8}$$

Equation 2.7 is similar to Sommerfield integral. An obvious observation is the decomposition of the spherical wave into cylindrical or conical waves. The wave mode decomposition property can be applied to the Hankel function of the first and second kind [Nowack, (2012)].

In general, the described characteristics makes Bessel beams very useful in various areas of science . For instance, the beam robustness property enables the beam to be used for optical trapping. In terms of free wave mode decomposition, the beams are assumed to have series of concentric rings which enables the carriage of energy between the rings and gives rise to a large propagating distance. The free wave mode decomposition property also enables Bessel beams to be used for seismology and geophysical reflective techniques. The decomposed spherical waves can be decomposed into a series of conical waves to either transmit, reflect or reverberate in layered mediums during geological probing [Chávez-Cerda, (1999)].

2.3 Orbital angular momentum (OAM)

Optical fields has angular momentum which can be classified into spin and orbital angular momentum. Spin angular momentum is associated with polarized light while orbital angular momentum is associated with the phase structure of the light. Beams with an azimuthal phase of $(\exp il\phi)$ carries orbital angular momentum, where l is the azimuthal indices and can have any integer number and ϕ is the azimuthal angle. Like the spin angular momentum with $\hbar k$ per photon, that of orbital angular momentum has $L = l\hbar$ per photon [Padgett et al., (2004)]. Figure 2.2 shows the helical phase front as a feature that describes a beam with orbital angular momentum in relation to its azimuthal indices.

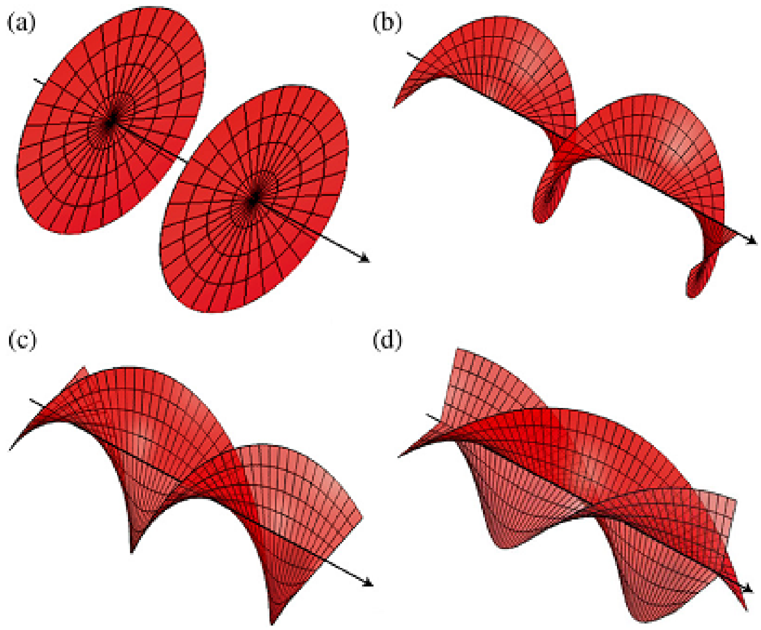

Figure 2.2: The helical phase front depending on the azimuthal indices (a) $l = 0$, (b) $l = 1$, (c) $l = 2$ (d) $l = 3$ [Padgett et al., (2004)].

For light beams having helical phase fronts, the azimuthal angle parameter produces an OAM which is parallel to the light beam axis during propagation. The beams contain optical vortex characteristics or phase singularities (null intensity and non-zero phase)

[Yao et al., (2011)]. These beams are usually called Laguerre-Gaussian (LG) modes. However, there are beams without helical phase dependence that can also carry OAM, example is the Hermite-Gaussian (HG) which is a product of a Hermite polynomial and Gaussian mode. As light propagates from a laser pump for instance, there is an expansion in the beams magnitude and phase at different position in its cross-section and these are usually described by mode functions. In the case of a cylindrical LG mode, it has an $\exp(-il\phi)$ phase factor and this is the feature that makes LG beams suitable for describing light beams which carry OAM [Padgett et al., (2004)].

2.3.1 Generating beams with orbital angular momentum

Some beam-type do not possess helical phase variation, such beams have spin angular momentum. Spin angular momentum related beams depends only on polarization, both HG and LG can have spin angular momentum. These beams are generated using quarter wave plate in the experimental setup. The quarter wave plates convert linearly polarized light into circularly polarized light [Trager, (2007)]. Other methods that can be used in generating beams with helical phase involves the use of microfabricated phase plate with a radial or azimuthal-type linear analyzer [Moh, K., et al, (2007)], segmented varying retarder [Lai, W. et al., (2008)], numerically computed holograms e.t.c. The method of microfabricated phase plate technique involves using a laser beam with circularly polarized beam alongside a fabricated plate. The obtained results yields a polarization which produces an axial symmetric and tightly focused beams. With a segmented spiral retarder, the technique involves converting a linearly polarized Gaussian beam into a radially polarized beam using a eight-segmented spiral varying retarder made from $\alpha-$ barium borate crystal. The obtained beam can be easily switched from radial to azimuthal vector beams.in the case of computer hologram, the holograms can generate several type of beams with desired OAMs. Figure 2.3 shows the generation of helical phase beams using digital holograms [Yao et al., (2011)]. In

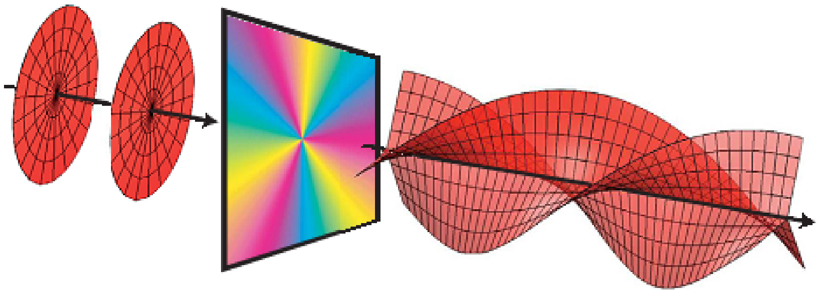

Figure 2.3: Illustration of the generation of helical phase beams using digital holograms encoded with $\exp(il\phi)$.

general, beams carrying OAM are perfect carriers of high-dimensional quantum information which makes such beams very useful in optical communications i.e their eigenstates in terms of photons are useful in quantum information processing.

2.4 Vector fields and their properties

Vector fields represents the optical fields lines propagating from a source which can be a diode laser pump. The vector fields have both intensity and phase. Another property of vector fields is its polarization.

Generally, optical fields can either be scalar or vectorial in nature depending on the state of polarization. Scalar fields possess spatially homogenous state of polarization. At different point in the scalar field cross section, the state of polarization of the fields remains unchanged. This property is basically the reason for characterizing scalar fields as partially or unpolarized optical fields [Wang et al., (2010)].

In the case where the state of polarization is spatially inhomogenous, a vector field is created. The field cross section can either be aligned in the radial or azimuthal direction. When the field cross section is aligned in the radial direction and applied to an object with high numerical aperture, the radially polarized vector fields can generate a strong longitudinal electric field in the central point of its focal plane. This property results in a tight focal spot. In the case of azimuthally aligned fields, the azimuthal vector field tend to have a hollow dark spot. This hollow dark spot is often referred to as vortex or singularity. At this vortex point, there is a zero intensity. Figure 2.4 illustrates the radial and azimuthal vector fields.

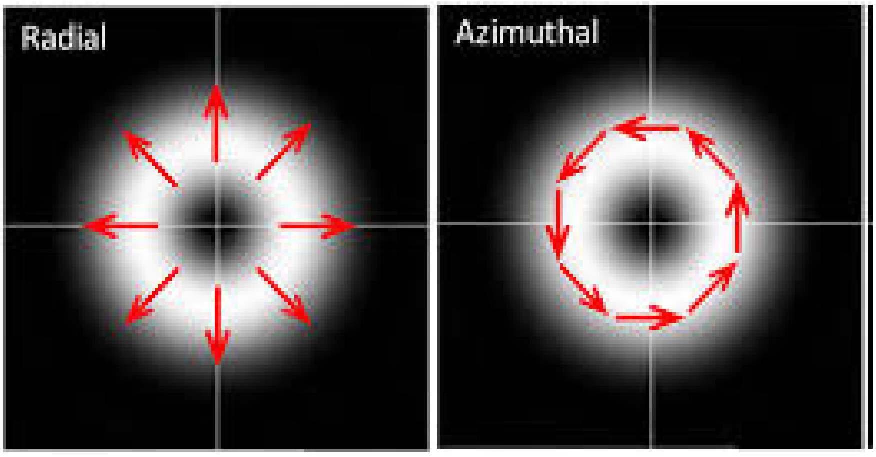

Figure 2.4: Illustration of a vector fields with alignment in the radial azimuthal direction.

As a result of the tight focusing feature of the vector fields, they are very useful in focusing applications such as optical 3D cage [Guo, Hanming, et al., (2011)]. Azimuthal vector fields having singularity at their central cross-section are also assumed to carry orbital angular momentum and applicable in optical information processing [Wang et al., (2010)].

2.4.1 Polarization of vector fields

Polarization of electric fields stems from vector fields which describes electric fields propagating along a distance. These electric fields are solutions to Maxwell homogenous equation with constant direction of propagation as depicted in equation 2.9 [Erikson and Singh, (1994)] as :

$$\nabla \cdot B = 0, \quad \nabla \times E + \frac{\partial B}{\partial t} = 0 \tag{2.9}$$

Most plane waves are either linearly (apex of the electric field oscillates in a line), elliptically (apex of the electric field moves on an ellipse) or circularly (with circular cross-section) polarized as shown in Figure 2.5[Iizuka, (2002)]. These forms of polarization are usually

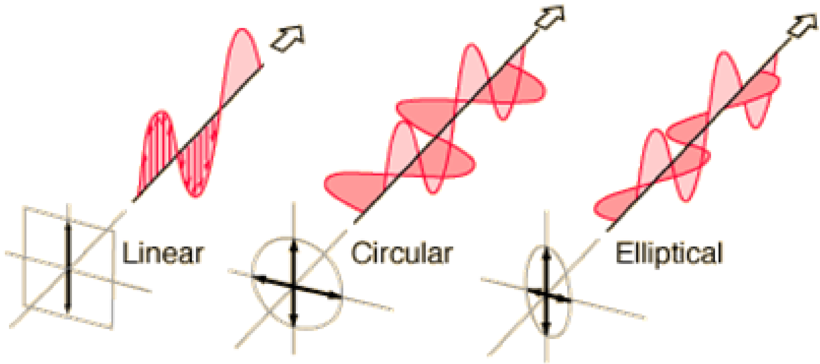

Figure 2.5: Different forms of scalar polarization of light : linear, circular and elliptical polarization respectively.

termed spatial (scalar) homogenous state of polarization. These states do not depend on the spatial direction of the beam cross-section (shape of the beam) [Zhan, 2009]. For a plane wave propagating in the z-direction, the electric field is given as:

$$\hat{E} = \hat{E}_0 e^{(ikz)} = \hat{E}_0 e^{\frac{i2\pi nz}{\lambda}} \tag{2.10}$$

Where $\hat{E}_0$ is a constant vector representing the amplitude of the wave at $z = 0$, n is the refractive index of the material of interest. If n is complex such that :

$$n = n_r + in_I \tag{2.11}$$

where n_r is the real part and n_I is the imaginary part. The imaginary part of n can be derived from extinction and absorption coefficient α given by :

$$\alpha = \frac{4\pi}{\lambda} n_I \tag{2.12}$$

the amplitude decreases exponentially and the wave equation becomes

$$\hat{E} = \hat{E}_0 e^{\frac{-\alpha z}{2}} e^{\frac{(i2\pi n z)}{\lambda}} \tag{2.13}$$

After a distance of $z = 1/\alpha$, the absolute value of energy $\left|\hat{E}\right|^2$ reduces to $1/e$ of the initial value. This means that the extinction of a plane wave can be accounted for by assuming a complex refractive index. The real part of the field accounts for the normal refractive properties of material of interest and the imaginary part account for absorption. If $n_I > 1$, then the wave only propagates through the material for a fraction of wavelength before the electromagnetic vector becomes negligible. This is an indication that polarization plays an important role in understanding the vector properties of light as it passes through materials [Trager, (2007)].

2.5 Cylindrical Vector (CV) Beams

Cylindrical vector beams are classes of vector beams possessing cylindrically symmetric (constant radius and angle inclination independent) electric field with radial and azimuthal polarization. These kind of beams satisfy the axial symmetry condition (unchanged if rotated around an axis) [Ito et al., (2010)]. Figure 2.6 is an illustration of the radial and azimuthal polarization state of a CV beam. The polarization state of CV beams has depedence on the alignment of the field. For instance, when the polarization of a beam is aligned in the radial direction, one have a radial polarization likewise having an electric field in the tangential direction which gives an azimuthal polarization [Beresna et al., (2015)].

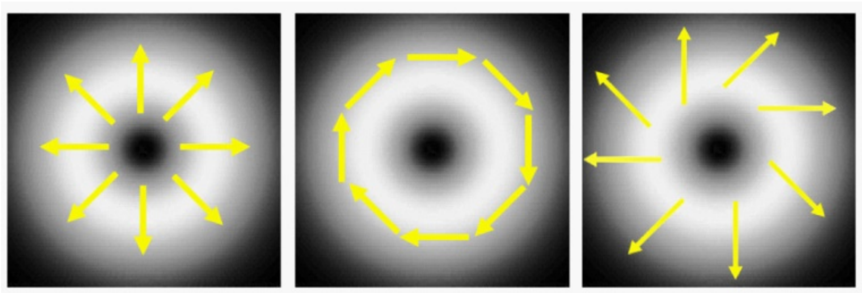

(a) (b) (c)

Figure 2.6: Diagram shows the distribution of polarized beams with (a) radially(b) azimuthally and (c)linearly superposition [Zhan, 2009].

Due to its cylindrical symmetric characteristics which gives a tight focused beam, CV beams have found use in practical applications such as imaging, machine particle trapping, data storage and sensing [Zhan, 2009].

CV beams are vector-beam solutions to Maxwell equations with axial symmetry in terms of amplitude and phase. Consider the scalar Helmholtz equations given as:

$$(\nabla^2 + k^2)E = 0 \tag{2.14}$$

and an electric field represented by the wave equation given as:

$$E(x.y, z, t) = u(x, y, z)\exp[i(kz - wt)] \tag{2.15}$$

Using the method of slowly varying envelope approximation, one can have

$$\frac{\partial^2 u}{\partial^2 z} \ll k^2 u, \qquad \frac{\partial^2 u}{\partial^2 z} \ll k\frac{\partial u}{\partial z} \tag{2.16}$$

Substituting 2.15 into 2.14 with some algebraic manipulations give

$$\frac{\partial^2 u}{\partial x^2} + \frac{\partial^2 u}{\partial y_2} + 2ik\frac{\partial u}{\partial z} = 0 \tag{2.17}$$

which leads to

$$\nabla^2 u - 2ik\frac{\partial u}{\partial z} = 0 \tag{2.18}$$

where $\nabla^2 = (\frac{\partial^2}{\partial x^2}) + (\frac{\partial^2}{\partial y^2})$ is the Laplacian operator and equation 2.18 is the Helmholtz equation from the paraxial limit. Equation 2.18 is not enough to describe the polarization of scalar and vector beams. The paraxial wave equations has solutions to the complete orthogonal basis for arbitrary paraxial beams which is the Hermite-Gaussian modes. With the slowly varying approximation, the Hermite-Gaussian mode U_{mn}^{HG} can be evaluated as:

$$U_{mn}^{HG} = N\frac{(1+it)^{N/2}}{(1-it)^{N/2+1}}H_m(\frac{\sqrt{2u}}{\sqrt{t^2+1}})H_n(\frac{\sqrt{2v}}{\sqrt{t^2+1}})\exp\left(\frac{-(u^2+v^2)}{(1-it)}\right) \tag{2.19}$$

Here, normalized coordinates are used i.e $u = x/w_0$, $v = y/w_0$ and $t = z/z_R$, N is the normalization constant, H_x denotes the Hermite polynomials, m,n are integers so that if N is the total order of the polynomials, then $m+n=N$. From this general Hermite-Gaussian mode equation, it is possible to compute the fundamental Gaussian mode equations with solutions that satisfy both scalar and vector polarization. Consider the Hermite differential equations given as:

$$\frac{d^2 H_m}{dx^2} - 2x\frac{dH_m}{dx} + 2mH_m = 0 \tag{2.20}$$

The general solutions for the Hermite differential equation is given as:

$$H_{m+1} - 2yH_m + 2mH_{n-1} = 0, \quad H_{m+1} + 2yH_m - 2mH_{n-1} = 0 \tag{2.21}$$

with set of polynomials of

$$H_0(y) = 1, \quad H_1(y) = 2y \tag{2.22}$$

In light of this, the Hermite-Gaussian mode HG_{mn} which is a solution satisfying equation 2.20 can be derived as:

$$u(x, y, z) = E_0(x, y, z)H_m H_n \frac{2}{w(z)}\sqrt{xy}\frac{w_0}{w(z)} \exp[-i\varphi_{mn}(z)] \exp\left[i\frac{k}{2q(z)}r^2\right] \tag{2.23}$$

Here $E_0(x, y, z)$ is the constant electric field amplitude, $w(z)$ is the beam size, w_0 is the beam size at the beam waist, $q(z)$ is the complex beam parameter given as $q(z) = (m + n + 1), \arctan \dfrac{z}{z_0}$ denotes the Guoy phase shift, $H_m(x)$ is the Hermite polynomial which satisfies the differential equation [Zhan, 2009]. In a situation where $m = n = 0$ and considering the set of polynomials, the solution becomes

$$u(r, z) = E_0\frac{w_0}{w(z)} \exp[-i\varphi(z)] \exp\left[i\frac{k}{2q(z)}r^2\right] \tag{2.24}$$

Equation 2.24 is the solution for a Gaussian beam with $\phi(z) = \arctan\left(\dfrac{z}{z_0}\right)$ which is the Guoy phase shift for Gaussian beams. Considering Laguerre differential equation given as:

$$x\frac{d^2L_p^l}{dx^2} - (l + 1 - x)\frac{dL_p^l}{dx} + pL_p^l = 0 \tag{2.25}$$

having associated solutions given as:

$$x(p) = e^{-p/2}p^l L_{\lambda-l-1}^{2l+1}(p) \tag{2.26}$$

In light of this associated solution and with cylindrical coordinate for beam-like paraxial solutions, a Laguerre-Gauss (LG_{pl}) mode can be derived as :

$$u(r,\varphi,z) = E_0(r,z)(\sqrt{2}\frac{r}{w(z)})^l L_p^l(2\frac{r^2}{w^2}(z))\frac{w_0}{w(z)}\exp\left(-\frac{kr^2}{2q(z)}r^2\right)\exp(-il\varphi) \tag{2.27}$$

where $L_p^l(x)$ denotes the Laguerre polynomials, $\varphi_{pl}(z) = (2p+l+1)\arctan\left(\frac{z}{z_0}\right)$ is the Gouy phase shift for $l = p = 0$. The solution also reduces to the fundamental Gaussian beam solution given as:

$$u(r,z) = E_0(r,z)\frac{w_0}{w(z)}\exp\left(-\frac{kr^2}{2q(z)}r^2\right) \tag{2.28}$$

These solutions 2.24 and 2.27 represents the paraxial beam-like solution which correlates to scalar beams.

For vector beams, consider the electric field wave equation given as

$$\nabla \times \nabla \times \vec{E} - k^2\vec{E} \tag{2.29}$$

Under paraxial slow-varying envelope approximations and considering cylindrical coordinates, one can have an equation that satisfies the equation 2.29 given as:

$$\frac{1}{r}\frac{\partial}{\partial}(r\frac{\partial U}{\partial r}) - \frac{U}{r^2} + 2ik\frac{\partial U}{\partial z} = 0 \tag{2.30}$$

with an axial symmetry (around the axis), one can have an electric field solution from equation 2.30 that is aligned in the azimuthal direction given as:

$$\vec{E}(r,z) = U(r,z)\exp(i(kz - wt))\vec{e_\varphi} \tag{2.31}$$

And in terms of azimuthal polarization symmetry, a trial solution can be assumed which is given as:

$$U(r,z) = AJ_1(\frac{\beta_r}{1+iz/z_0})\exp\left(-\frac{i\beta^2 z/(2k)}{1+iz/z_0}\right)u(r,z) \tag{2.32}$$

where $u(r,z)$ is the fundamental Gaussian solution as given by equation 2.24, J_1 is the first order Bessel function of the first kind. β is a parameter with constant magnitude [Forbes, (2014)]. The solution given by equation 2.32 is a correlation to an azimuthally polarized vector Bessel-Gaussian beam solution. Similarly, one can obtain a transverse magnetic field solution that is given by :

$$\vec{H}(r,z) = -BJ_1(\frac{\beta_r}{1+iz/z_0})\exp\left(-\frac{i\beta^2 z/(2k)}{1+iz/z_0}\right)u(r,z)\exp(i(kz-wt))\vec{h}\varphi \tag{2.33}$$

The solution given in equation 2.33 is aligned in the radial direction which indicates radial polarization for electric fields. However, the electric field has a very weak z-component and under paraxial conditions, it can be neglected . Figure 2.7 is a representation of the modes for linearly polarized electric field (a)-(f) as well as radial and azimuthally polarized electric fields (g) and (h). The linearly polarized fields are generally termed spatial homogenous polarized as they have uniform polarization distribution across the beam. The case of azimuthal and radial have non-uniform polarization distribution.

CV beams can be generated in several ways. As illustrated in Figure 2.8, combining two linearly polarized Hermite-Gaussian laser beams interferometrically as described by

$$\vec{E_r} = HG_{10}\vec{e}_x + HG_{01}\vec{e}_y, \qquad \vec{E_\varphi} = HG_{01}\vec{e}_x + HG_{10}\vec{e}_y \tag{2.34}$$

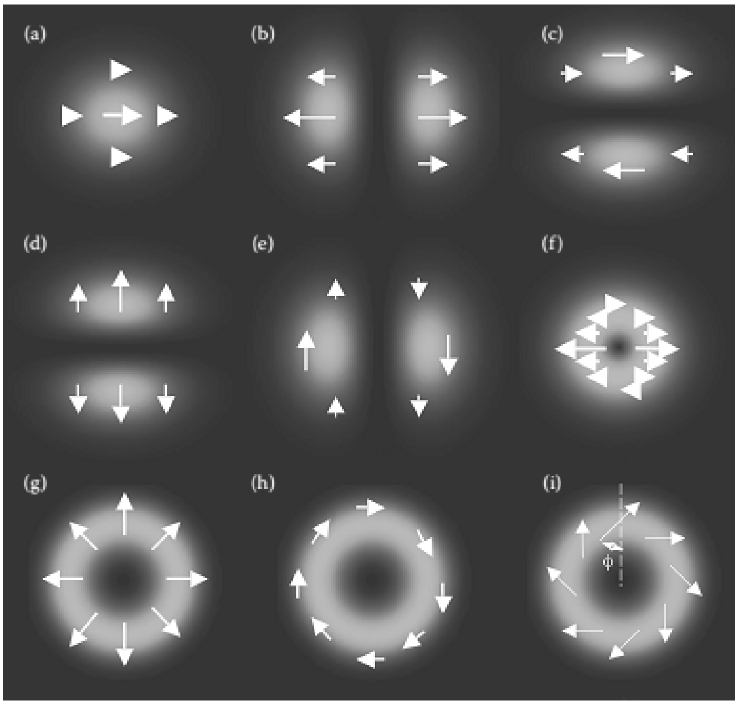

Figure 2.7: Illustration showing the different modes that is possible with linearly polarized Hermite-Gauss, LG electric fields [Forbes, (2014)].

or by transmitting a linear polarized light beam through a nematic liquid crystal. Insertion of optical elements such a Quarter wave plate into a laser resonator can also generate CV beams [Woerdemann, 2012].

2.6 Bessel beams (BBs)

Sequel to the work of Durnin, Bessel beams exhibit cylindrical symmetry with plane electromagnetic wave behaviour. With strong conviction, BBs are said to satisfy the conditions of cylindrical vector beams [Durnin et al., (1987)].

Bessel beams can either be scalar or vectorial in nature. In scalar form, BBs exhibit spatial homogeneous behaviour which has been described earlier (linear, elliptic and circular polarization) [Bouchal, 2003]. BBs in the scalar regime involve mostly superposition of transverse electric (TE) modes and transverse magnetic (TM) modes and interferences of

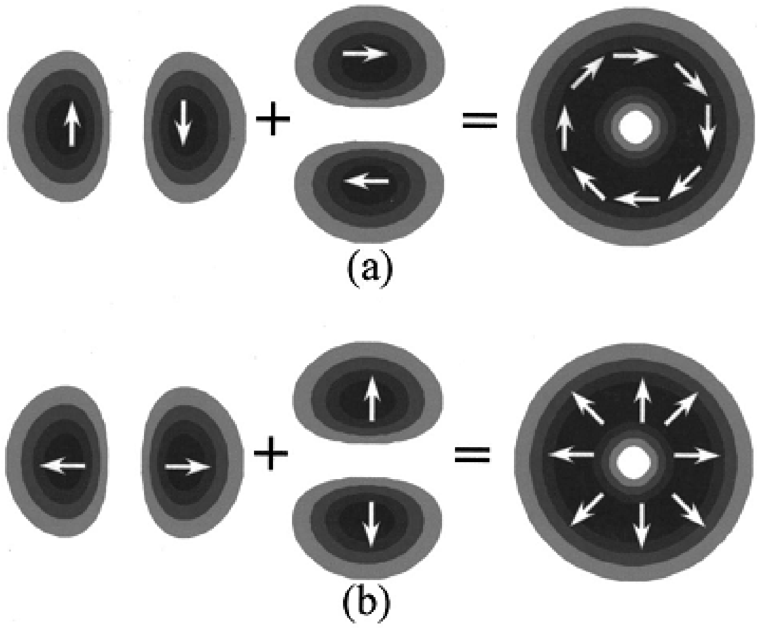

Figure 2.8: Diagram shows the combination of two linearly polarized optical fields which results in the production of azimuthal and radial polarized fields (CV) beams.

linearly polarized plane waves which produces complex energy fluxes that are very useful in various applications [Bouchal, 2003]. Basically, Vector Bessel Beams are light beams with a spatial inhomogeneous state of polarization possessing radial or azimuthal polarization as described above in polarization section [Dudley et al., (2013)]. The electric field describing a $l - th$ order Bessel beam is expressed as:

$$E_l(r, \phi, z) = A \exp(ik_z z) J_1(k_r r) \exp(il\phi)$$

Here, A is the amplitude of the beam, J_1 is the first order Bessel function, k_z and k_r are the longitudinal and radial component of the wave-vector respectively where $k = \dfrac{2\pi n}{\lambda} = \sqrt{k_z^2 + k_r^2}$. The Bessel function behaves differently in various scenarios, for example, in the the zeroth order, the output beam has a central maximum bright spot. Furthermore, in other cases of higher order Bessel beam, the beam has a zero-on- axis intensity (dark central spot)that is surrounded by rings which is due to phase singularity of l-parameter as depicted in the azimuthal phase term ($il\phi$). [McGloin and Dholakia, (2005)].

The mathematical function which describes the behaviour of Bessel beams (Both scalar and vector BBs) are solutions which satisfies Bessel's differential equation. There are different approaches that can be used in computing the solutions, a few are explored as follows:

Solution from wave equation Consider the wave equation given as:

$$\nabla^2\psi = \frac{1}{c^2}\frac{\partial^2\psi}{\partial t^2} \tag{2.35}$$

a scalar, azimuthally symmetric wave with frequency w propagating in the z direction is a solution satisfying equation 2.35 and is given as :

$$\psi(r,t) = f(\rho)\exp[i(k_z z - wt)] \tag{2.36}$$

where $r = \sqrt{x^2+y^2}$, Substituting the second derivative of $\psi(r,t)$ of equation 2.36 into 2.35 gives :

$$\frac{d^2 f}{d\rho^2} + \frac{1}{\rho}\frac{df}{\rho d\rho} + (k_f^2 + k_z^2) \tag{2.37}$$

Equation 2.37 is in form of the differential equation for Bessel function of order 0 and the solution can be written as :

$$f(\rho) = J_0(k'\rho) \tag{2.38}$$

where

$$k_f^2 = k' + k_z^2 \tag{2.39}$$

Introducing an arbitrary real parameter α into equation 2.39 will yield $k' = k_f \sin\alpha$ and $k_z = k_f \cos\alpha$ and one can have the expected cylindrical wave form given as:

$$\psi(r,t) = J_0(k'\rho)\exp[i(k_z z - wt)] = J_0(k_f \rho \sin\alpha)\exp[i(\cos\alpha z - wt)] \tag{2.40}$$

Equation 2.40 is the usual Bessel beam equation. From $w = ck_z/\cos\alpha$ The constant α is in the z-direction and it is the angle that describes the superposition of the infinite plane waves that leads to Bessel beams [Mcdonald, (2000)].

Solutions from vector potential Consider the scalar wave equation given as:

$$\nabla^2 E(\boldsymbol{r},t) - \frac{1}{c^2}\frac{\partial^2}{\partial t^2}E(r,t) = 0 \tag{2.41}$$

where ∇^2 is the laplacian operator, c is the speed of light in free space, r is the position vector. With angular frequency w, Electric field $E(r,t)$ can be written as:

$$E(r,t) = E(r)\exp^{(iwt)} \tag{2.42}$$

Substituting 2.42 into 2.41, one obtains :

$$\nabla^2 E(r) + k^2 E(r) = 0 \tag{2.43}$$

This is the usual Helmholtz wave equation with wave number $k = w^2\mu_0\varepsilon_0$. Using the variable seperable method in cylindrical coordinate, equation 2.42 becomes

$$E(r,t) = E_0(r,t)J_n(k_\perp \rho)\exp(in\varphi)\exp(i(k_z z - wt)) \tag{2.44}$$

Here $E_0(r,t)$ is a constant, J_n is the nth-order Bessel function of the first kind. $\rho = \sqrt{x^2+y^2}$, $x = \rho\cos\varphi$, $y = \rho\sin\varphi$ and $k^2 = k_\perp + k_z^2$ being the radial and longitudinal wave numbers respectively. Hence the time-averaged intensity can be calculated as:

$$I(\rho,\varphi,z \geq 0) = I(\rho,\varphi,z=0)|E_0 J_n(k \perp \rho)|^2 \tag{2.45}$$

And as it is observed, the intensity distribution is constant which describes the robust characteristic of Bessel Beams [Mcdonald, (2000)].

2.7 Summary

This chapter described the characteristics of Bessel beams. Bessel beams are characterized by robustness, phase dislocation, free-wave mode propagation e.t.c, Bessel beams are also cylindrically symmetric in nature. the mathematical implications presented in this chapter indicates that the beams can either be scalar or vectorial in nature. Bessel also show potential in carrying orbital angular momentum and this is emphasized in the $L = l\hbar$ that is carried by each photon of the beams. Bessel beams can be linearly polarized depending on the radial or azimuthal alignment direction of the fields. The polarization of the beam can be converted easily from linear to circular polarization using wave plates.

Chapter 3

Generation and detection of Scalar Bessel Beams

3.1 Introduction

The generation of Bessel beams poses a challenge due to some factors such as infinite energy and propagation distance. An alternative resolution is generating a quasi-Bessel beams which have the same characteristics as BBs with finite propagation distance. A few of the methods are described in this section

Axicon method: Axicons methods for generation of Bessel beams is one of the most efficient technique amongst the known techniques. Figure 3.1 illustrates the method of the Axicon in generating Bessel beams. A conical lens (Axicon) is used to channel the

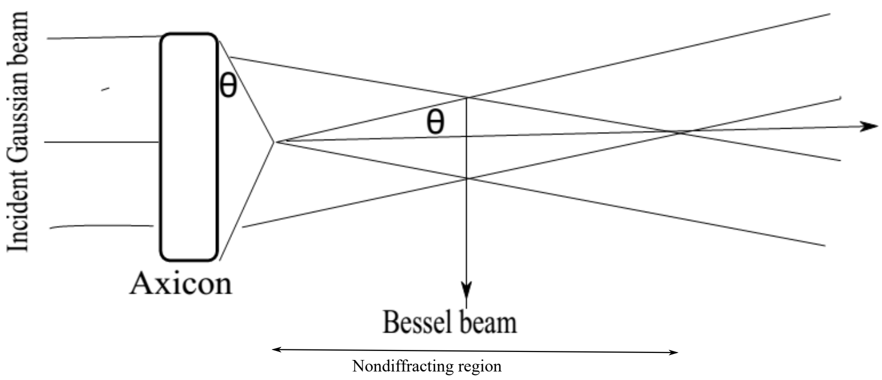

Figure 3.1: Description of the generation of Bessel beams using an axicon. The inclinatiion angle is approximately equal to the Axicon open angle. The nondiffracting region is the distance where the beams are formed.

entire input beam towards the centre of the lens. Since there is no bending of light in the middle of a lens, the beams can propagate easily across that path without diffracting [Duocastella and Arnold, (2012)].

The Gaussian beam represents the incoming wave that is incident on the Axicon. The inclination angle is usually very small ($\approx 0.5^0$) and approximately equal to the Axicon opening as represented in the Figure 3.1. The output beam is a Bessel mode profile [**?**]. Furthermore, other methods such as using an azimuthal phase beam by spatial light modulators or a Laguerre-Gaussian (LG) beam can be utilized in generating Bessel beams. Figure 3.2 is a description of the procedure for generating Bessel beams using LG beams. With

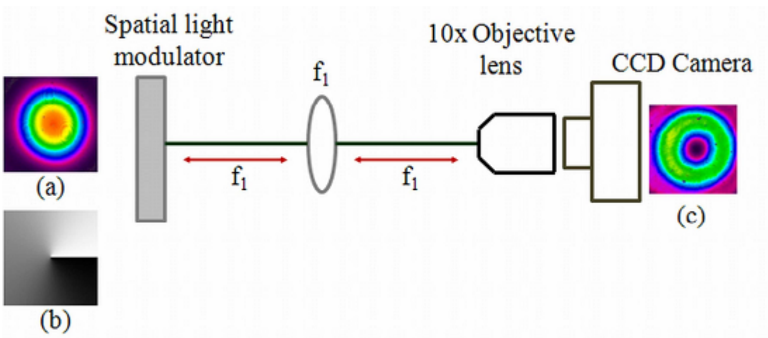

Figure 3.2: Illustration of the procedure for the generation of Laguerre-Gaussian beams, the CCD camera is used to record the generated beam (Ismail, 2012).

reference to Figure 3.2, a Laguerre-Gaussian beam (a modified Gaussian beam) of radial and azimuthal index l with zero order is used to illuminate a conical Axicon which produces BBs of order l. The setup is the same as the previous, the only difference is the input beam. The key advantage here is that higher-order BBs can be generated due to the orbital angular momentum carrying potential of LG beams. This can be seen in the azimuthal phase terms l dictates the amount of OAM that is carried by the beam [Dudley et al., (2013)]. The procedure involves firstly generating LG beams by channeling a Gaussian beam into a spatial light modulator with a relevant grey scale pattern as indicated in Figure 3.2(b). Some of the experimental results are shown in Figure 3.3. From Figure 3.3, it is observed that an

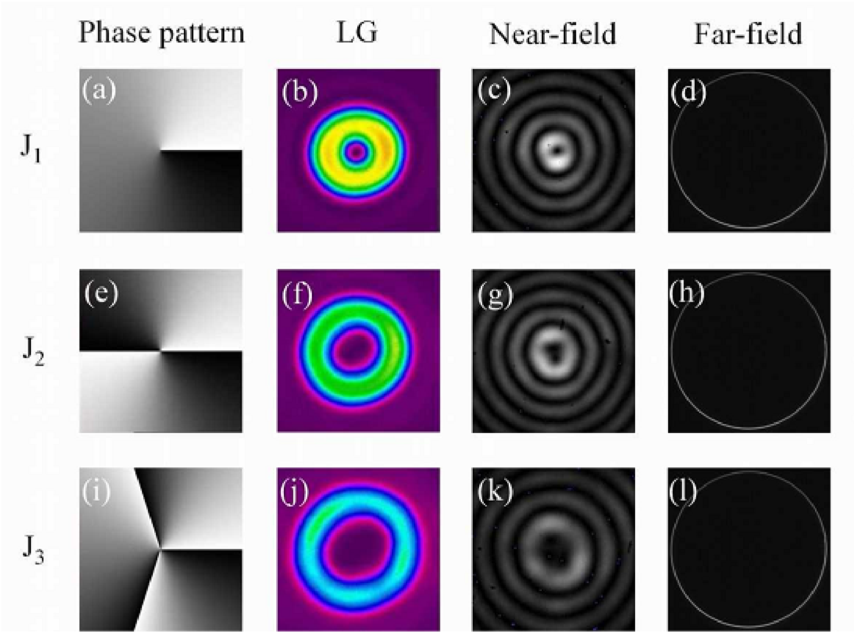

Figure 3.3: Illustration showing the generated images of several higher-order Bessel beams using LG beams [Ismail et al., (2012)].

increase in the topological charge of the LG beams causes a corresponding increase in the near-field topogical charge of the generated BB. It is worth noting that higher order BBs can propagate in a finite distance having an annular ring at the far-field intensity profile [Ismail et al., (2012)].

Aperture method: The aperture method is actually the method implemented by Durnin in 1987. Here an annular slit is placed in the back of the focal plane of a lens that converges the incident light. Figure 3.4 is an illustration of how BBs are generated using the aperture method. When the input beam is illuminated on it, it narrows it to the centre. Though BBs are produced in the process, the aperture blocks most of the radiated incident light thereby leading to low efficiency of the beam produced [Duocastella and Arnold, (2012)].

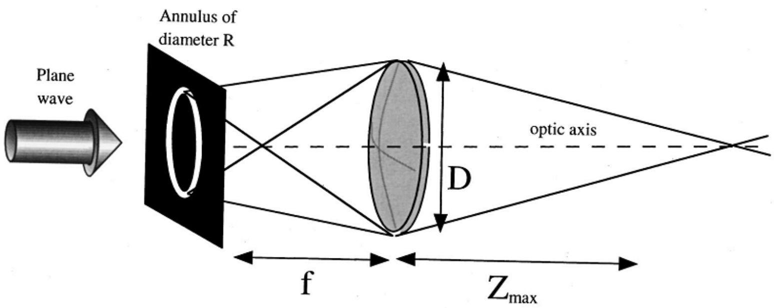

Figure 3.4: Description of how Bessel beams are generated using apertures in redirecting the incident beam.

Tunable Acoustic Gradient (TAG) lens: Here an acoustic signal is generated in a circular piezoelectric liquid compartment which in turn gives a sinusoidal refractive index in the device. If a cylindrical compartment is used, then the refractive index takes the form

$$n(r,t) = n_0 + n_A J_0(r)\frac{wr}{v}\cos(wt) \tag{3.1}$$

with n_0 being the static refractive index, w-frequency, v is the speed of sound in the fluid and n_A is the constant that varies with the physical characteristics of the medium (lens size, driving voltage amplitude, mean density) with value in the order of 10^{-5}. As soon as the compartment is illuminated with light, the refractive index profile transforms the light into multiscale BBs with a central beam and surrounding Bessel-like rings [Tsai et al., (2006)].

3.2 Spatial light Modulators(SLM)

As earlier noted in section 3.1, the energy of the Bessel beams depends mostly on the intensity of the beam which is a function of the amplitude and phase of the beam. There are different optical devices that can modulate the intensity of input beams, however, one device that is recommended is the Spatial Light Modulators (SLMs). SLMs are digital, programmable optical devices that help to vary the input property (amplitude and phase) of a light beam according to a fixed spatial pixel format [Duocastella and Arnold, (2012)].

An SLM comprise mainly of a liquid crystal display (LCD) with several pixels. Each pixel is addressed by two electrodes in a way that the molecular component of the pixels aligns in parallel to the electrodes. When an electric field in the form of light beam is applied to thin electrodes, the molecules respond by tilting in the direction of the field. The response causes the refractive index experienced by the light to alter the phase of the incident light beam [Lazarev, Grigory, et al,(2012)]. SLM imparts a phase profile into an incident beam such that the modulated phase profile of the beam appears to have an orthonormal set which serves as a channel for carrying optical information.This optical nformation can be encoded into an SLM in the form of a filter and applied to a laser beam. This encoded information in the SLM can be propagated to a desired distance where it is needed [Bouchal and Celechovský, (2004)]. SLMs come in different types such as phase only, amplitude and coupled phase and amplitude modulated types depending on the intended use. As the name-type implies, beam modulation in terms of the amplitude, phase or both can be implemented accordingly [Ambs et al., (2007)].

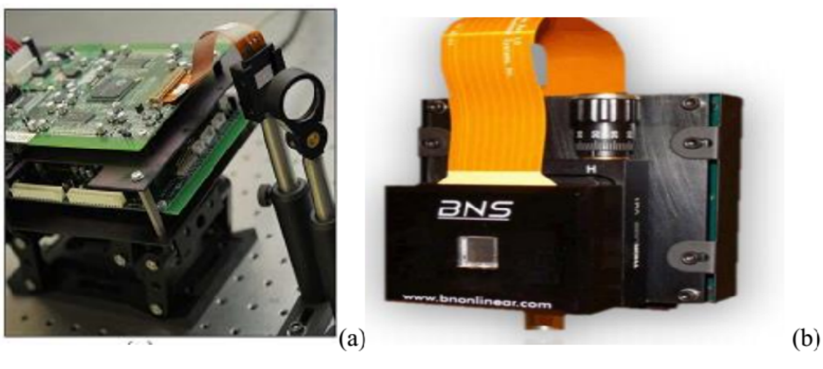

Figure 3.5: (a) Diagram showing the inclusion of an SLM as an optical element (b) picture showing a liquid crystal SLM.

Figure 3.5 shows a typical example of a phase only SLM alongside its inclusion in an optical experimental setup. The non diffracting property of BBs ensures that the information generated at the SLM is recovered at the desired destination without loss of intensity.

3.2.1 Computer generated holograms (CGH)

Computer generated holograms forms the backbone behind SLMs. Basically, holograms records the interference of two coherent (fields with equal intensity and phase) fields i.e an object and a reference wave field. The object field represents the wave that is observed when an object of interest is illuminated by light. The reference wave on the other hand is the plane wave that is stored in the recording medium [López-Mariscal and Gutiérrez-Vega, (2007)]. When an object field reaches the recording medium such as a photographic film or CCD

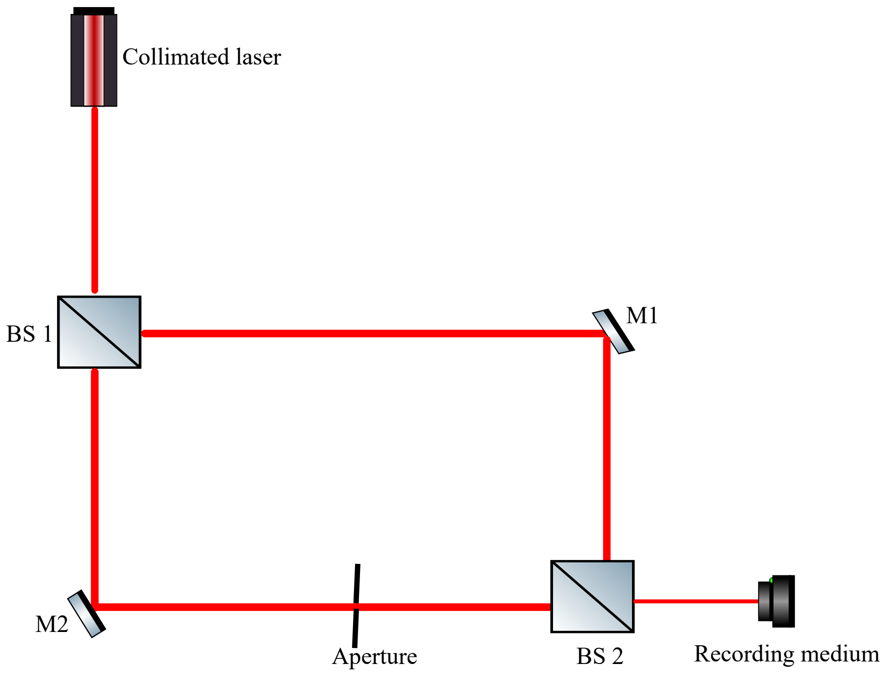

Figure 3.6: A simple optical setup describing the principle behind holography capturing of a light field through an aperture. BS-beam splitter, M- mirrors.

camera, the variation in the intensity of light at the plane of the recorder is stored. This intensity comprises the phase and amplitude of the object field [Poon and Liu, (2014)]. Figure

3.6 shows the working principle of the hologram. In this simple setup, a beam splitter reflects and transmits a light plane wave. One of the plane waves illuminates a pinhole aperture and the other is received by a mirror and both light waves are received at the recording medium i.e the interference of the object and reference fields [Poon and Liu, (2014)].

3.2.2 Calibration of Spatial light Modulators

The spatial phase distribution of an SLM in terms of the parameters (grey level of the image display of the device) controlling the input signal need to be verified experimentally. This is to ensure the uniformity of the phase response of the SLM as well as addressing errors that are mostly due to voltage independence. Avoiding errors such as this can improve the image performance of the SLM [Martínez-León et al., (2009)]. The relevance of SLMs relies mostly on producing a precise amplitude and phase modulation independently in each addressable pixel. For instance, a liquid crystal whose exact modulation depends on the polarization of the incident and transmitted light beams modulates the input beam without prior information of the input beam. As a result of the unknown polarization, the calibration of the spatial light modulator is necessary [Ferreira and Belsley, (2010)]. There are several ways to calibrate SLMs. Figure 3.7 shows a simple method for calibrating SLMs [Ferreira and Belsley, (2010), Martínez-León et al., (2009)].

3.2.3 Phase only modulated SLM for Bessel Beams

The phase modulation of a Bessel beam can be implemented using holograms. In the implementation process, parallel-aligned TN-LC (SLM of choice) is used to generate holographic phase gratings which enables the beam generation [Chattrapiban et al., (2003)]. Usually, the SLM is not used directly but connected in the experimental setup as an optical

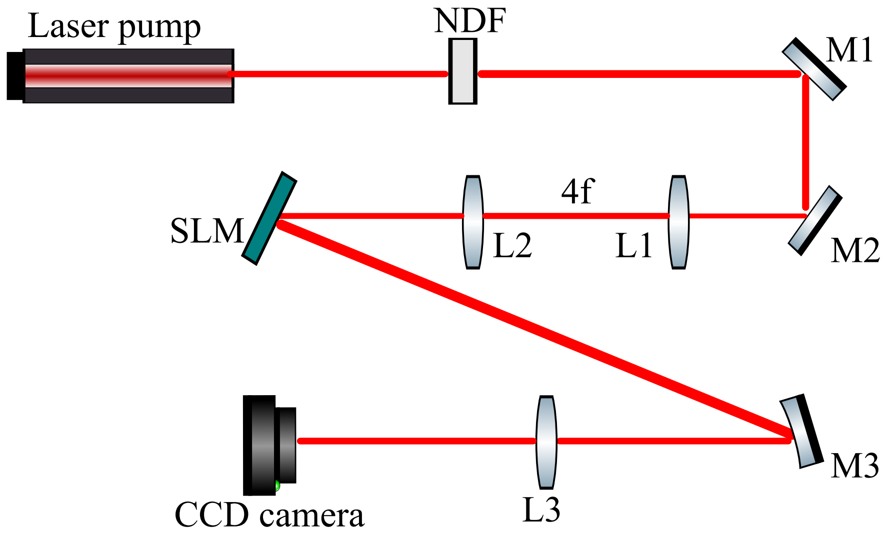

Figure 3.7: Schematics of the setup used for the calibration of a Spatial light modulator, L-lenses, M- mirrors, NDF- neutral density filter, SLM-spatial light modulator.

element. Although the SLM can be programmed directly with the relevant phase profile $\phi(x, y)$ there exist imperfections. These imperfections are represented as undesired beams appearing as sets of beams resulting to superposition of diffraction orders. The introduction of phase gratings helps to overcome this issue as it creates an angular deviation between the diffraction orders. This enables a spatially filtered position in the Fourier plane of the SLM to choose the first-order diffraction beam [Leach et al., (2006)]. To generate a Bessel beam, the phase of the hologram image is programmed to be

$$\phi(r) = k_r \tag{3.2}$$

where $\beta = k_r$ is the diffractive angle. This is related to the phase of the Axicon by

$$(n-1)\alpha = \frac{\beta}{k_0} \tag{3.3}$$

where α is the Axicon angle. Bessel beams generated from this hologram set up will have a phase $\phi = \beta k_r$ which indicates that the size of the central spot. 3.8 is an illustration showing an experimental procedure for generating Bessel beams using phase only SLMs . The function of the neutral density filter is to ensure adequate intensity of light is received at the detection point [Leach et al., (2006)]. The advantage of this method is the flexibility

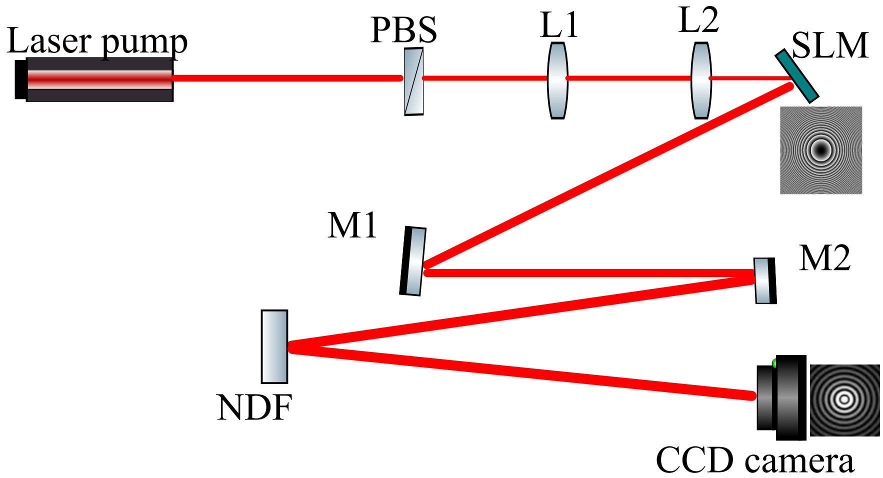

Figure 3.8: Generation of phase modulated BBs using spatial light modulators, NDF-neutral density filter ensures adequate intensity of light is received at the detection point.

of increasing or decreasing the amount of azimuthal charge that can be programmed into the SLM.

3.2.4 Amplitude and Phase variation of Bessel Beams Using Spatial Light Modulators

Another application of SLM in terms of Bessel beam generation is its ability to modulate the amplitude and phase of a Bessel beam simultaneously. Figure 3.9 illustrates the working principle of simultaneously varying the amplitude and phase of Bessel beams using SLMs. The polarization direction of the input beam is set to 45^0 with reference to the $x-$ axis. Figure 3.10 is a graphical illustration that depicts the procedure involved in the amplitude and phase modulation using two SLMs. With the first SLM having a phase distribution $\varphi_1(x, y)$. The beam after the first SLM becomes half modulated with distribution $x-$ axis of $\frac{\sqrt{2}}{2}A_0$ and $y-$ axis $\frac{\sqrt{2}}{2}A_0 \exp(i\varphi_1(x, y))$. With the polarizer inclined

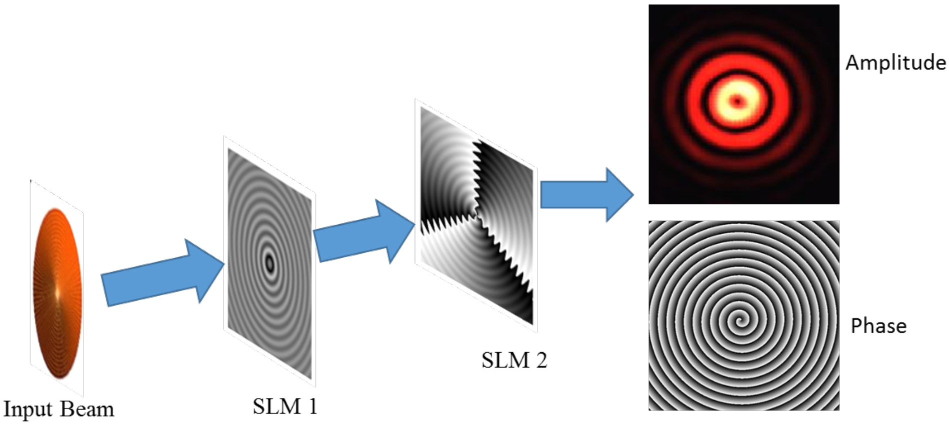

Figure 3.9: Schematic diagram showing the working principle of modulating amplitude and phase of a Bessel beams using spatial light modulator. The polarization of the field is paramount in the setup and this is achieved using a polarizer.

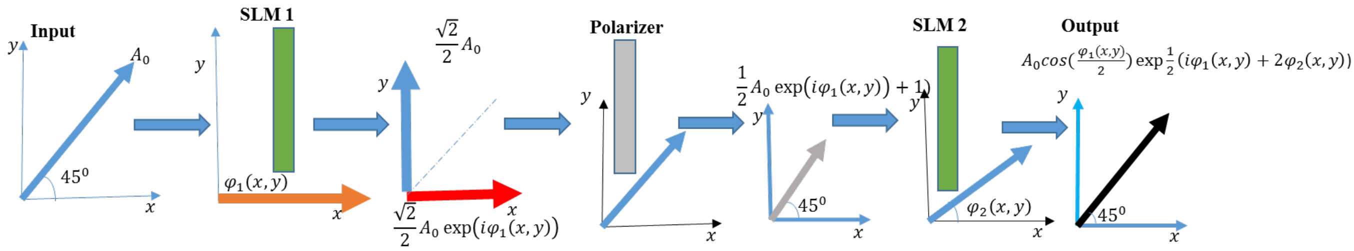

Figure 3.10: The principle behind the modulation of amplitude and phase of an input beam with an initial phase of $\varphi_1(x, y)$. The polarizer ensures the angle of the propagating beam. The output field indicates a modification of both the amplitude and phase of the input field.

at 45^0 with respect to the $x-$ axis, the field becomes:

$$E(x, y) = \frac{\sqrt{2}}{2} A_0(\exp(i\varphi_1(x, y))) \times \frac{\sqrt{2}}{2} + \frac{\sqrt{2}}{2} \times \frac{\sqrt{2}}{2} = A_0(\exp\left(\frac{i\varphi_1(x, y)}{2}\right) + 1) \quad (3.4)$$

When the light propagates after the polarizer through the second SLM with phase distribution, a field with a modified amplitude and phase is obtained . The idea is to allow a polarized light at 45^0 with respect to the horizontal (x) direction with a phase distribution $\varphi_2(x, y)$ to propagate through the second SLM. The output field becomes:

$$E(x, y) = \frac{1}{2} A_0(\exp(i\varphi_1(x, y)) + 1) \exp(i\varphi_2(x, y)) = A_0 \cos\left(\frac{\varphi_1(x, y)}{2}\right) \exp i(\frac{\varphi_1(x, y) + 2\varphi_2(x, y)}{2}) \quad (3.5)$$

where $\varphi_1(x, y)$ denotes the amplitude after the first SLM and $\varphi_1(x, y) + 2\varphi_2(x, y)$ describes the new phase of the beam after the second SLM. From this information, varying the phase information written on both SLMs can invariably change the amplitude and phase of the beam separately and concurrently [Zhu and Wang, (2014)].

3.3 Generating Bessel Beams Using digital Axicons and annular rings

Several methods have been proposed by researchers on how to create BBs using spatial light modulators. This can be done by encoding phase distribution of the wave front of propagating beam to generate desired beam [Birch et al., (2000)]. A few of these methods are described in this section.

3.3.1 SLM and Axicons

Basically, an Axicon is a conical lens that can be used to generate Bessel beams. A general purpose lens can generate a focal point however, an Axicon can generate focal lines that can extend along reasonable distance from millimeters to kilometers depending on the desired design [Guo-qin et al., (1996)]. As mentioned earlier in section 3.1, an Axicon consists of a glass cone which creates conical wavefront forming a narrow focal line. The intensity of the beam generated by the Axicon can be varied depending on the shape of the Axicon [Guo-qin et al., (1996)]. The light rays incident behind the Axicon is refracted towards the optical axis at almost the same angle for all the rays. The interference of the incident rays at the optical axis produces a tight focal line defining the region where Bessel beams are formed [Burvall et al., (2005)]. The opening angle θ of the cone is given by :

$$\theta = (n-1)\gamma \tag{3.6}$$

Given the beam width w_0, the length of the non-diffracting region of the Bessel beams can be calculated as :

$$Z_{max} = w_0/\theta \tag{3.7}$$

and usually, the Bessel beams are found at the point $Z_{max}/2$ and what is observed after the Z_{max} region are just conical waves.

In terms of Bessel beam generation using digital axicon i.e modulating the phase of a beam with an SLM. Consider the Axicon schematics shown in Figure 3.11. The transfer

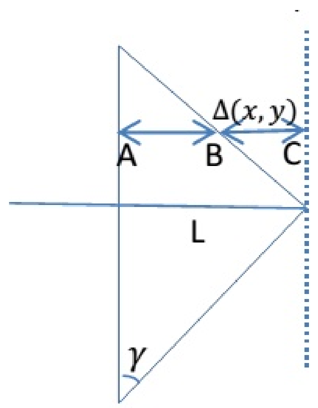

Figure 3.11: The schematical representation of an Axicon with a phase function of position.

function (function that modifies the initial light field) is given as:

$$\tau(x,y) = \exp(i\phi(x,y)) \tag{3.8}$$

where $\phi(x, y)$ is the phase function of position and is given as :

$$\phi(x, y) = k\Delta(x, y) + kn(L - \Delta(x, y)) \tag{3.9}$$

$\Delta(x, y)$ is the distance between B and C. With reference to 3.11, the distance is given as:

$$\Delta(x, y) = \tan\gamma\sqrt{x^2 + y^2} = r\tan\gamma \tag{3.10}$$

Assuming the thickness L of the axicon is very small, it can be ignored so that :

$$\phi(x, y) = k(n - 1)r\tan\gamma - knL \tag{3.11}$$

and the transfer function becomes:

$$\tau(x, y) = \exp(ik(n - 1)r\tan\gamma) \tag{3.12}$$

Accounting for the OAM modes of the beam, a topological charge l and a phase ϕ parameter can be included such that :

$$\tau(x, y) = \exp(ik(n - 1)r\tan\gamma) + l\phi \tag{3.13}$$

the transfer function of the Axicon can be rewritten in terms of a phase functions for simplicity and is given as:

$$\tau = \exp i(r/r_0) \tag{3.14}$$

where r denotes the cross-section of the cone and r_0 represents a set of parameters and is given as :

$$1/r_0 = k(n-1)\tan\gamma \tag{3.15}$$

where n is the refractive index of glass with $k = 2\pi/\lambda$ being the usual wave number and λ the wavelength of laser beam. Figure 3.12 is a simple setup for generating Bessel beams using the phase of an Axicon.

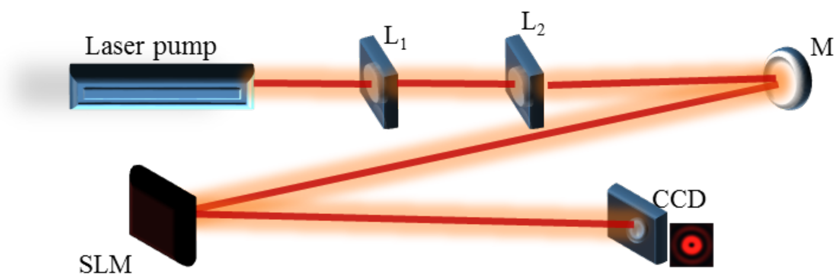

Figure 3.12: Bessel beam generation using a digital axicon with a spatial light modulator M-mirror, SLM- spatial light modulator, L1 and L2 are lenses used for expanding the beam width, CCD-camera.

3.3.2 Annular ring and SLM

The Durnin experiment is the method described earlier in section 3.1. The combination of the annular slit and SLM involves implementing the Durnin's ring-slit experiment digitally. The ring slit is encoded into the SLM in the form of a hologram. Ideally, the Bessel beam is assumed to be a Fourier transform of a ring. Figure 3.13 shows the principle behind the ring-slit method. The ring is placed at a focal plane behind the lens which generates the beam as shown in Figure 3.13 and illuminated with an optical field (Gaussian beam). After the illumination, each wave front along the slit becomes a coherent source point producing a new field as a result of the transformation from the lens lying on the conical plane [McQueen et al., (1999)].

Implementing this approach with an SLM is not complicated. The ring is as-

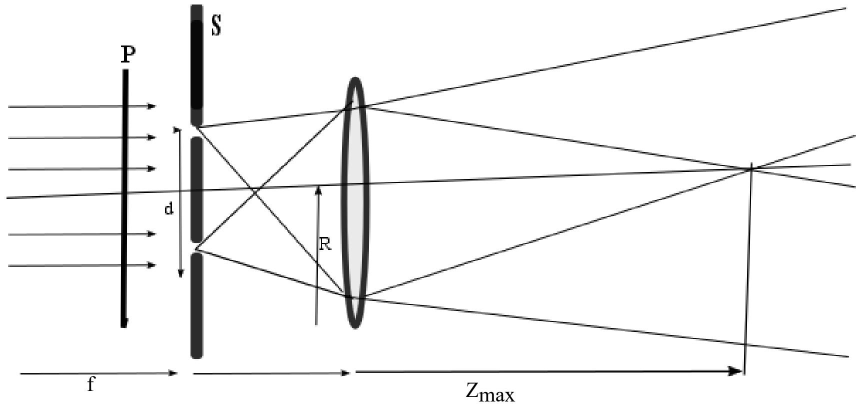

Figure 3.13: The generation of Bessel beams using a ring slit, S-aperture, d-diameter of the incident beam, R-radius of the converging lens in the focal plane with propagation region Z_{max}.

sumed to be two with different radius and the SLM is illuminated with a Gaussian beam [Dudley et al., (2013)].

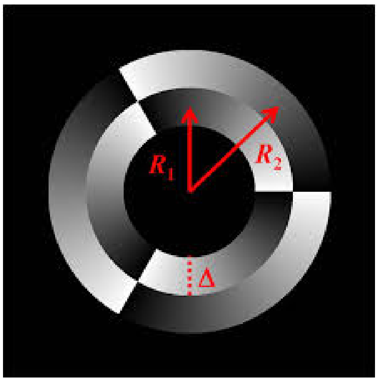

Figure 3.14: Illustration of the ring slit that is illuminated by the initial light beam, the ring is divided into two radii R_1 and R_2 respectively.

The digital ring-slit takes the form of a transfer function that describes the slit. In this case, the function is given as:

$$\tau(r,\phi) = \begin{cases} \exp(il\phi) & \text{if } R_1 - w/2 \leq r \leq R_1 + w/2 \\ exp(-il\phi) & \text{if } R_2 - w/2 \leq r \leq R_2 + w/2 \\ 0 & elsewhere \end{cases} \tag{3.16}$$

Where R_1 and R_2 are the radii of the inner and outer ring-slits respectvely and w is the width of the rings, ϕ is the azimuthal angle and l is the azimuthal mode index. The experimental setup for the generation is shown in (Figure 3.15).

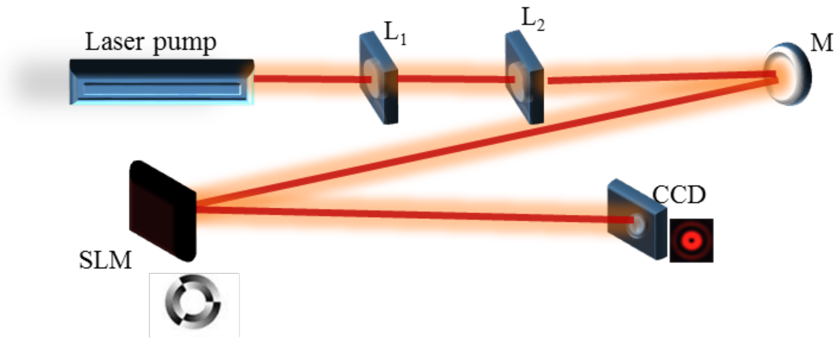

Figure 3.15: Generation of Bessel beams using a hologram of a ring-slit, M-mirror, SLM-spatial light modulator, L-lenses.

3.4 Modal Decomposition (MD)

In BBs generation, one task is to generate the beams and another task is to analyze the profile of the generated beam. Laser beams are optical fields which are superposition of modes which has complex expansion coefficient. Modal decomposition measures the over lap of the beam profiles with other beam modes [Schulze et al., (2012)].

The proven method to sorting optical field content is modal decomposition. Modal decomposition involves the description of optical fields in terms of their eigenmodes or into a superposition of orthonormal basis function. MD characterizes the beam in terms of its phase structure, phase singularity [Kaiser et al., (2009)]. Knowing the characteristics of an optical field will not only help to identify the beam but would also help to classify the use of the light beam.

The usefulness of modal decomposition of light is seen in various avenues of scientific research. It is particularly useful in classical field of science, quantum information processing

[Ourjoumtsev, A. et al.,(2006)], fibre optics systems [Kaiser, T., Schröter, S. and Duparré, M, (2009)] and laser resonator systems [Schmidt, A., et al.,(2011)].

The earliest method for modal decomposition involves direct modal description (DMD) of an optical field by analyzing the field using mathematical formalism. DMD emphasizes the physical principle of optical fields and how it correlates with the theoretical background of the fields [Kaiser et al., (2009)]. However, the set-back of this method is that the fields are difficult to analyze and the beam-type information is supposed to be known for the analysis to be effective. As such, the method is not reliable. A more reliable method is the SLM and the fourier transform lens technique. The SLM and fourier lens system implements an inner product that maps all necessary information about the field into one dimensional set of coefficients.

3.4.1 Spatial light modulators and Fourier Transform Lens Technique

Different numerical methods have been used by different researchers to characterize optical fields. SLM alongside a lens is used to decompose the orbital angular momentum spectrum of an optical field [Dudley et al., (2013)] .

An arbitrary optical field can be considered as a superposition of basis functions. These functions can be expressed as mode functions. Each mode has a weighting coefficient which maps the relevant information about the optical field into a sets of 1-dimensional coefficients. The objective of modal decomposition is to determine the weighting coefficients.

Consider an optical field expressed as:

$$U(r) = \sum_{n=1}^{n_{max}} c_n \psi_n(r) \tag{3.17}$$

where c_n depicts the unknown coefficient of the optical field and $\psi_n(r)$ is the mode function. The mode function $\psi_n(r)$ can be written in terms of orthonormal property as:

$$\langle \psi_n | \psi_m \rangle \iint d^2 r \psi_n^*(r) \psi_m(r) = \delta_{nm} \tag{3.18}$$

where the integral is over $\mathbb{R}^2$. The unknown coefficient can be found using :

$$c_n = \rho_n \exp(i \Delta \phi_n) = \langle \psi_n | U \rangle \tag{3.19}$$

where ρ_n^2 is the modal weights and $\Delta\phi_n$ is the phase of the optical field [Schulze et al., (2012)]. This technique can be extended to modes describing Bessel beams. Considering the basis of a Bessel beam having mode defined by:

$$U_l(r, \phi, z) = \sqrt{\frac{2}{\pi}} J_l(\frac{z_R k_r r}{z_R - iz}) \exp(il\phi - ik_z z) \exp\left(\frac{i w_0^2 k_r^2 z - 2kr^2}{4(z_R - iz)} \right) \tag{3.20}$$

where l is the azimuthal topological charge, $J_l(\cdot)$ is the Bessel function of the first order, k_r is the transverse wave number, k_z is the longitudinal wave number, w_0 is the Gaussian beam radius and z_R is the Rayleigh length given by :

$$z_R = \frac{\pi w_0^2}{\lambda} \tag{3.21}$$

The Bessel beam mode can be expanded as

$$g(r,\phi) = \sum_{l\to\infty}^{\infty} \int_0^{\infty} c_l(k_r) u_l k_r(r,\phi,0) dk_r \tag{3.22}$$

where $g(r,\phi)$ is the complex amplitude of the Bessel beam at $z = 0$, $c_l(k_r)$ is the unknown expansion function that can be found by the inner product measurement experiment. Figure 3.16 is the setup for implementing the modal decomposition of an optical field using an SLM and fourier lens [McLaren et al., (2013)].

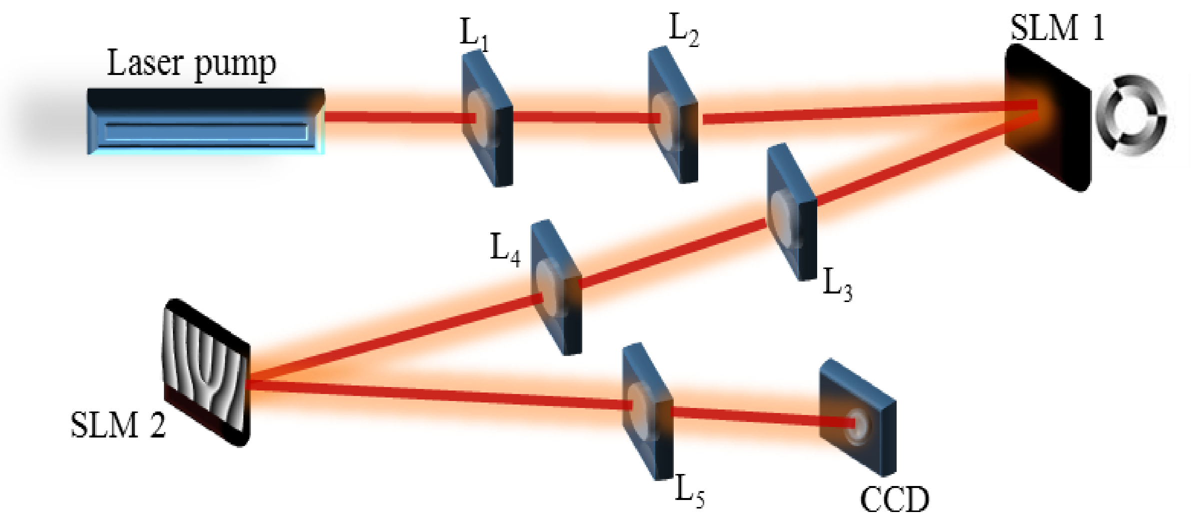

Figure 3.16: Description of the experimental setup that enables the decomposition of an optical field using an SLM.

Here, the generated Gaussian beam was passed through a 5× magnified zoom telescope and allowed to pass through a liquid display of SLM 1. The output beam from SLM 1 was a Bessel beams profile. The Bessel fields are magnified with another lens 10 times and passed through another SLM2 for the modal decomposition process. the inner product is implemented with a match filter that is set to $\exp(il\phi)$. The detection point is observed after the fourier lens $L5$. The holograms that is encoded on both SLMs can be altered accordingly to modify the intensity of the beams. This method can easily be applied to other vortex beams for unraveling the OAM contents of the beam.

3.5 Experimental generation and detection of Scalar Bessel beams

Equation (3.13) was used to generate the holograms shown in Figure 3.17. The hologram was encoded onto the SLM for the Bessel beam generation. As earlier noted about

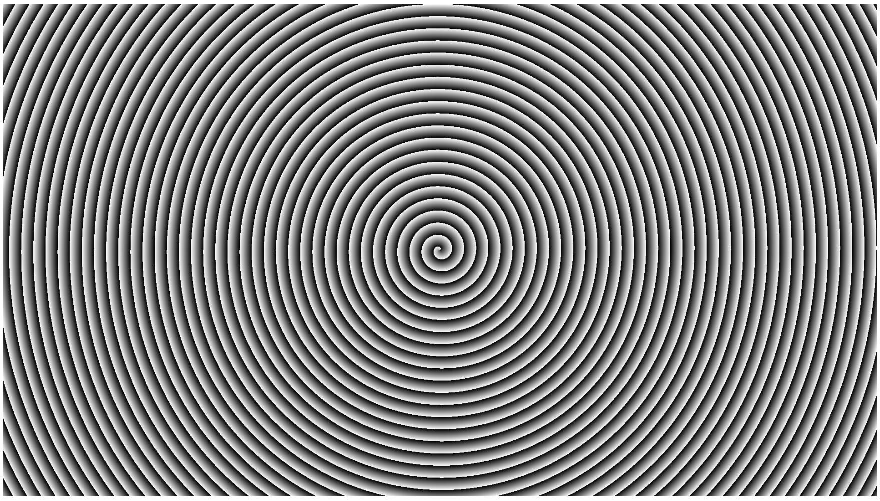

Figure 3.17: The hologram used for the generation of the scalar Bessel beams using the phase of an Axicon

using the Axicons to generate Bessel beams is the nondiffracting beam region. This length is the range where the Bessel beams are observed as described in the Figure 3.18. Although beams appearing as BBs can be observed before and after this region, these beams are conical waves. The length of the region usually denoted as Z_{max} is calculated using

$$Zmax = \frac{w_0}{(n-1)\gamma} \tag{3.23}$$

where w_0 and γ describes the beam radius $(\frac{w_0}{2})$ and Axicon angle respectively. n is the refractive index of glass. In this calculations, the beam width was chosen to be 1 mm,

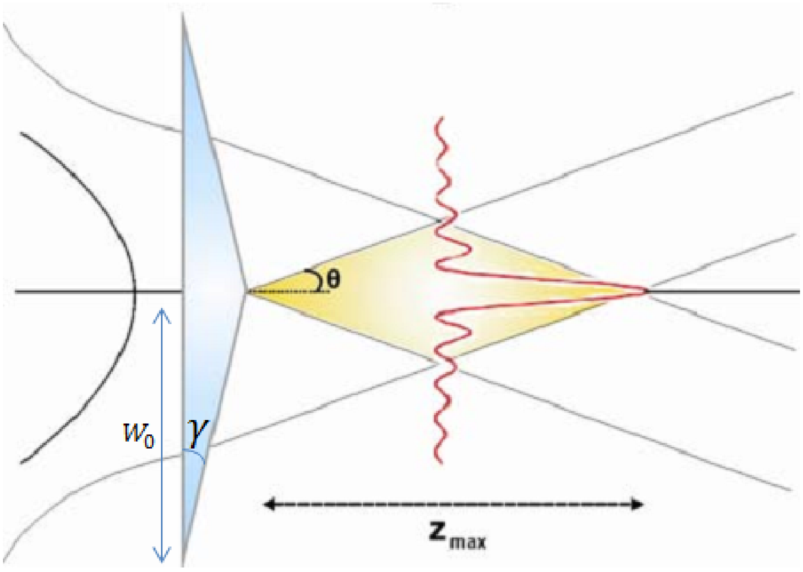

Figure 3.18: An illustration of an Axicon which describes the non-diffracting finite region where the Bessel beams are formed.

$n = 1.5$ and Axicon angle $\gamma = 0.2$. The non-diffracting region in this case was calculated to be $\approxeq 14$ cm.

3.5.1 Experimental setup for scalar Bessel beams

The experimental set up used for the generation of the beams is shown in Figure 3.19. The setup comprises of a HeNe laser source ($633nm$), a spatial light modulator (SLM) (Holoeye, PLUTO-VIS with 1920 x 1080 pixel and calibrated for a 2π phase shift at $633nm$, aligning mirror, a polarizer and a CCD camera. The scalar Bessel-Gaussian beam was generated by propagating a Gaussian beam through the SLM. An aperture was introduced (not shown in the experimental setup) in-between the 4f lens system to filter out the zero and second diffraction order beams and the output was eventually captured by the CCD camera.

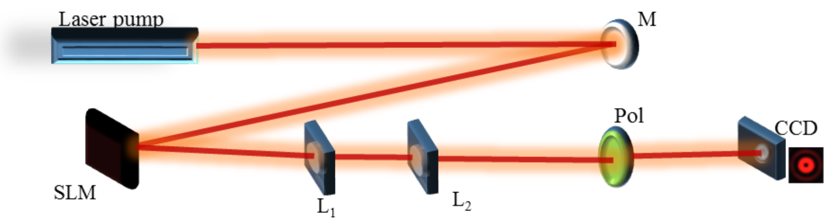

Figure 3.19: Experimental setup for the generation of the scalar Bessel beam using digital axicons. M-mirror,$L1 = 200$ mm, $L2 = 200$ mm SLM-spatial light modulator, CCD-camera, Hene-Gaussian beam laser source.

3.5.2 Results and discussion for scalar Bessel beams

The generated scalar BBs are shown in Figure 3.20. 3.20(a) illustrates a zero-order Bessel beam with a bright spot. 3.20 (b)-(k) are higher order Bessel beams with dark spot otherwise called donut beams.

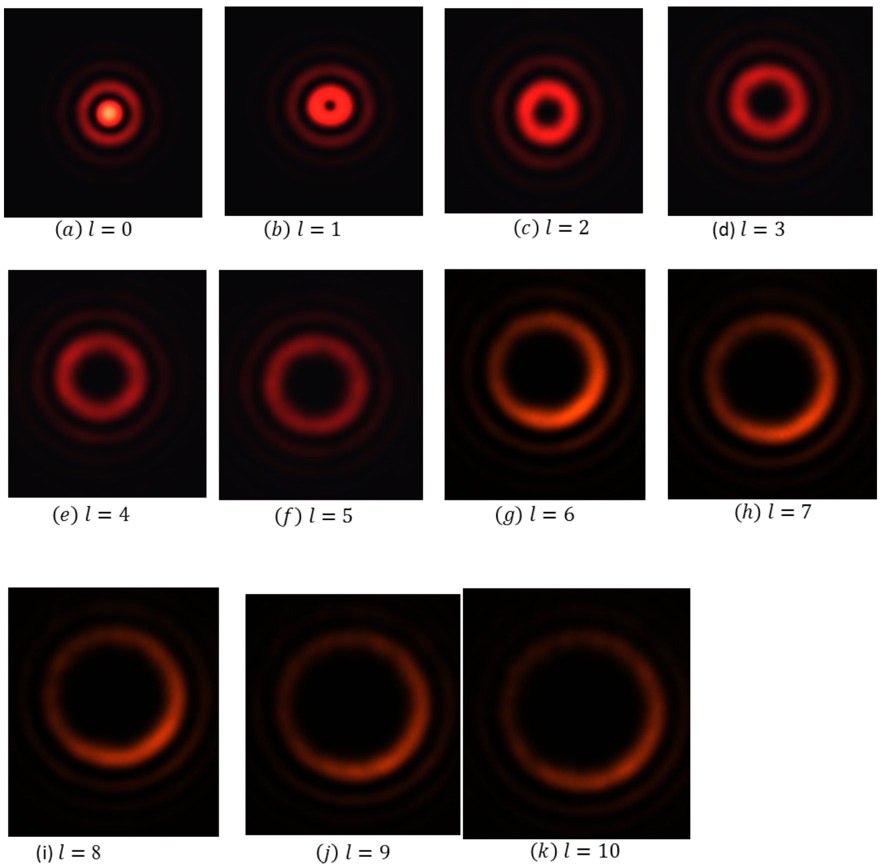

Figure 3.20: Experimentally generated Bessel-Gaussian beam with topological charge varying from $l = 0$ to $l = 0$.

Next, a polarizer was introduced to obtain the different polarization state of the beams between 0 and 2π.The OAM focus was on $l = 1$ mode. The decision to restrict the experiment to $l = 1$ was due to the fact that the same result is observed for different OAM modes of the scalar beams as illustrated by Figure 3.21. Regarding the higher order

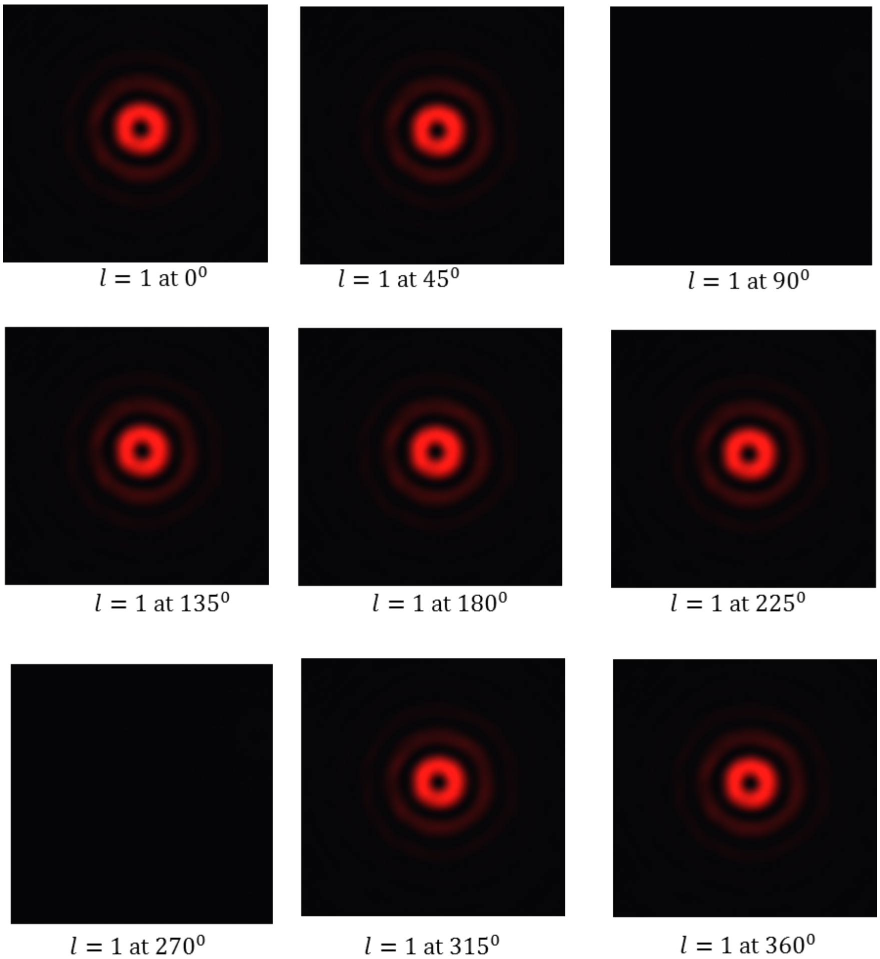

Figure 3.21: The different polarization state of $l = 1$ Bessel-Gaussian beam between 0 and 2π.

Bessel beams, the topological charge increase have a corresponding increase in the vortex singularity which describes the increase in the order of Bessel beams. The intensity profiles for $l = 0$ to $l = 2$ are shown (figure 3.22) The obtained intensity profiles of the generated beams were captured in accordance to the calculated non-diffracting region of $(\frac{1}{2}Z_{max})$. It is worth noting that the increase in the topological charge creates room for an increase in the OAM content of the beam. Furthermore, it was observed that for several angles of

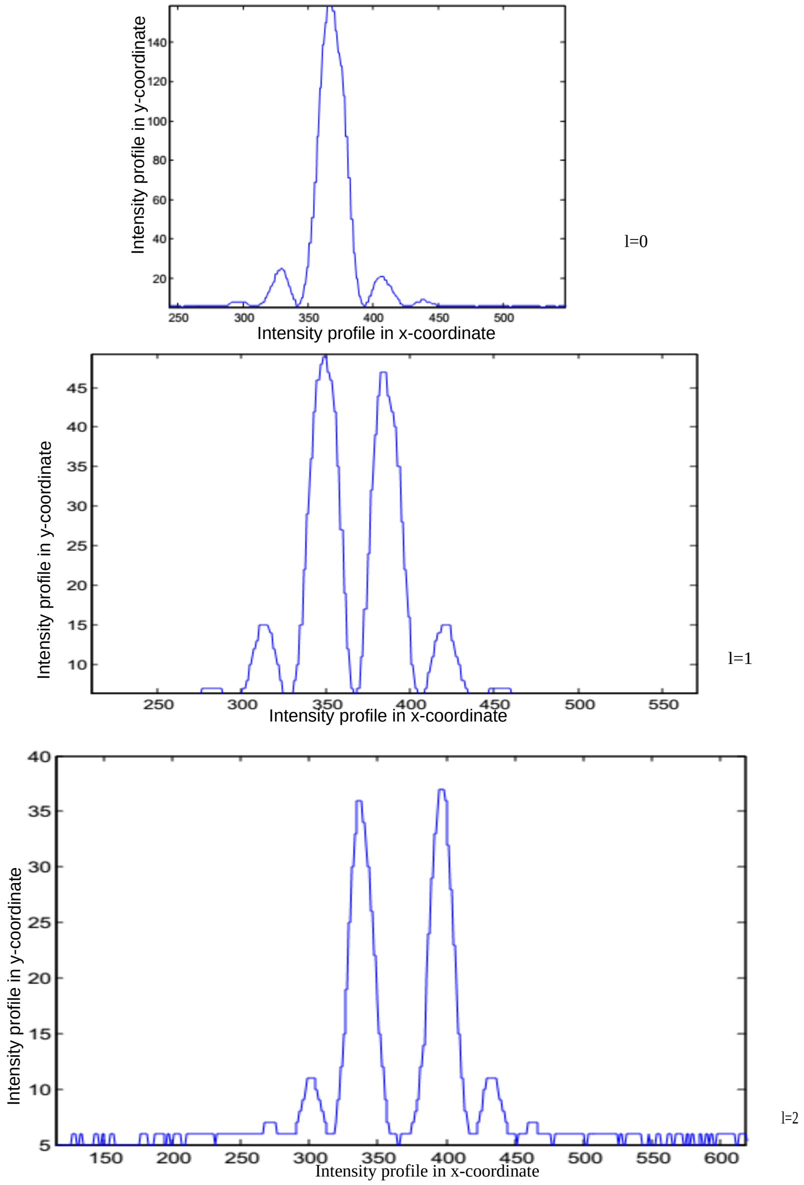

Figure 3.22: The plot of intensity profile of the generated zero-order and higher order Bessel-Gasussian as by the CCD at $\frac{1}{2}Z_{max}$.

polarization between 0 and 2π, the shape of the beam remains unchanged, this is because the Bessel beams are considered partially polarized and such, insignificant effect is observed with the insertion of the polarizer. Furthermore, in the case of 90^0 and 270^0 position of the Bessel beam, there was no beam detected. This is because, the beam after the polarizer was not horizontally polarized but vertical and as a result no beam was observed at the detection point.

It is also important to note that the generated Bessel beams are z-dependent. This means that when the axicon angle γ is increased, it has a corresponding effect on the non-diffracting region. In this case, when the axicon angle γ was increased from $\gamma = 0.2$ to $\gamma = 0.36$, the non-diffracting region reduced from 28 cm to $\approx$ 16 cm however, the shape and the intensity of the beam remains invariant.

3.6 Detection of scalar Bessel beams

As discussed earlier, modal decomposition involves the process of unpacking an optical field in terms of OAM or modal content. It helps to determine the power content and the phase of the modes contained in the optical field.

An optical field denoted by $U(r, \phi)$ can be written in terms of an orthogonal basis function as:

$$U(r, \phi) = \sum_{l=1}^{\infty} c_l \psi_l(r, \phi) \tag{3.24}$$

where $r = (x, y)$, denotes the spatial coordinates, c_l is the expansion coefficient and ψ_l describes the lth vector mode of the optical field. The intensity (power) of the field can thus be measured from the initial field $U(r, \phi)$ by:

$$I(r) = |U(r)|^2 \tag{3.25}$$

where $|U(r, \phi)|^2 = \langle \psi_l^* | \psi_l \rangle$. The "*" symbol indicates the complex conjugate of the field ψ_l. The technique used in this case was identical to the method described in section 3.4.1. The inner products was implemented by encoding two transfer functions of opposite signs. The transfer functions used in the inner product measurement as depicted in equation 3.25 are given as:

$$\psi_l = k(n-1)\gamma \exp(il\phi), \quad \psi_l^* = k(n-1)\gamma \exp(-il\phi) \tag{3.26}$$

The experimental setup used in the implementation is shown in Figure 3.23. ‘ A $4f$ lens

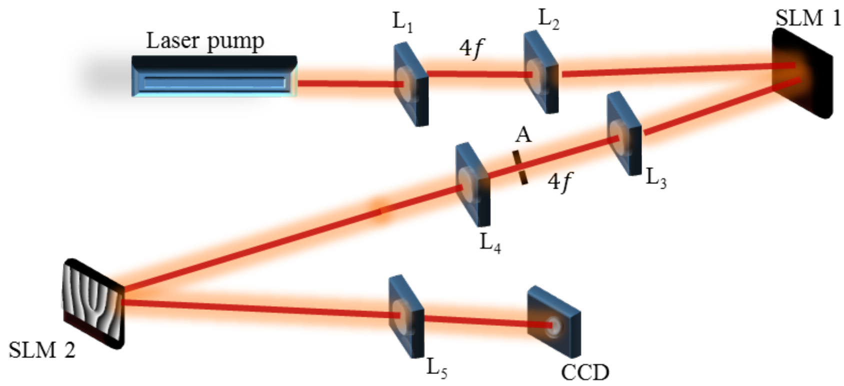

Figure 3.23: Setup used for the modal decomposition of the scalar Bessel beams, SLM-spatial light modulator, M-mirrors, L-lenses, $L1 = 200$ mm, $L2 = 200$ mm, $L3 = 100$ mm, $L4 = 100$ mm, $L5 = 300$ mm, Pol-Polarizer, A-aperture, CCD-camera.

system was used to image the generated BG beam back into the second partition of the SLM for the inner product measurement. Another lens $L5 = 300$ mm is used to perform a fourier transform of the modes generated by the decomposition and the results are captured by the CCD camera.

3.6.1 Results and discussion for detection of scalar Bessel beams

The intensity plots as captured by the CCD camera are shown in Figure 3.24. When a Gaussian beams is incident on an Axicon, a Bessel beam is produced and if the process is reciprocated, a Gaussian beam is produced. The high peak indicates the bright on-axis intensity of the reciprocated process as indicated in the plot. The topological charge values or modes ranged from -5 to 5 and it was observed that when an input mode matches the correlation filter that was implemented, a bright on-axis intensity was observed and that is indicated by 1 in the plot and zero intensity was observed for other cases when there is a

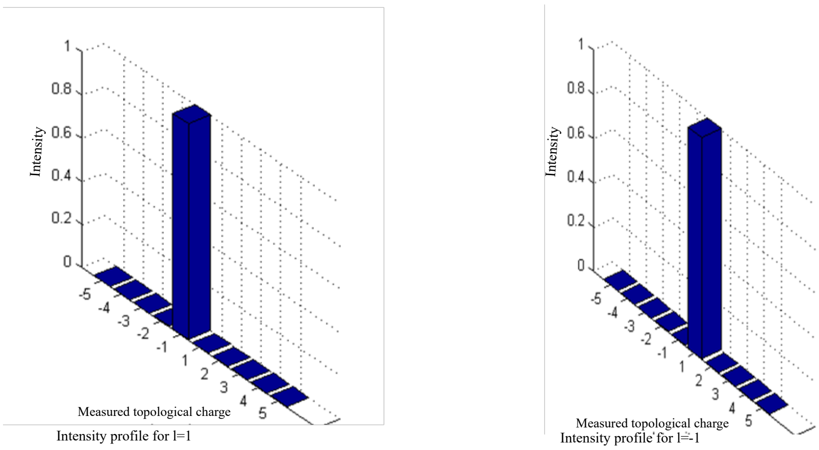

Figure 3.24: The intensity plots of the implementation of modal decomposition of the scalar Bessel-Gaussian beams.

mismatch.

3.7 Summary

Axicons and annular slits are some of the conventional ways to generate Bessel beams. Digitally implementing this method is not only convenient but also very efficient as issues that involves misalignment of the Axicon and the blocking of some the input beams are avoided. Although Spatial light modulators do not solve the problem of misalignment however, they proffer an efficient technique for generating Bessel beams. The generated Bessel beams in this case are zero-order Bessel beams with a bright spot and donut beam in the case of higher order Bessel beams. SLMs are also used to detect the OAM modes that are embedded in the higher order modes of the generated beams. The obtained results indicates that an OAM mode of $l = 1$ is inherent in the beam and other higher modes can be obtained as well using the same technique of spatial light modulators and fourier lens transform.

Chapter 4

Generation and Detection of Vector Bessel beams(VBBs)

4.1 Introduction

Generation of vector Bessel beams involves converting linearly polarized beams to circularly polarized beams. Vector beams has a coupling of spatial modes and polarization. Several optical devices such as dielectric metasurfaces, q-plates e.t.c are used for the generation of vector beams however, focus is given to q-plate in this research work. Q-plates are briefly introduced with their working principle. This is followed by the experimental setup, results and discussions.

4.2 Q-plates

Optical fields have some inherent rotational characteristics that are embedded in the electromagnetic nature of the field. This electromagnetic nature is described in terms of twist and spin. Spin describes the rotation of the electric and magnetic field oscillating within the optical field (circular polarization), a twist, on the other hand, describes light that has fork-shaped wavefront. optical fields having this nature can be assumed to have angular momentum. There are several methods for generating this sort of light fields but the most convenient and efficient method is to use the q-plate [Kwok et al., (2013)] . The q-plate enables the interaction between spin and twist of optical fields.

Q-plates can also be used to convert spin angular momentum (SAM) to orbital angular momentum (OAM) within a propagating optical field. Q-plates introduces OAM to an ordinary light beam having linear polarization as described in Figure 4.1 [Marrucci et al., (2011)] and also used in the generation of vector-vortex light beams. These beams have different sets of OAMs and uniform polarization. These vortex beams have various applications, one of which is quantum information processing [Cardano et al., (2012)].

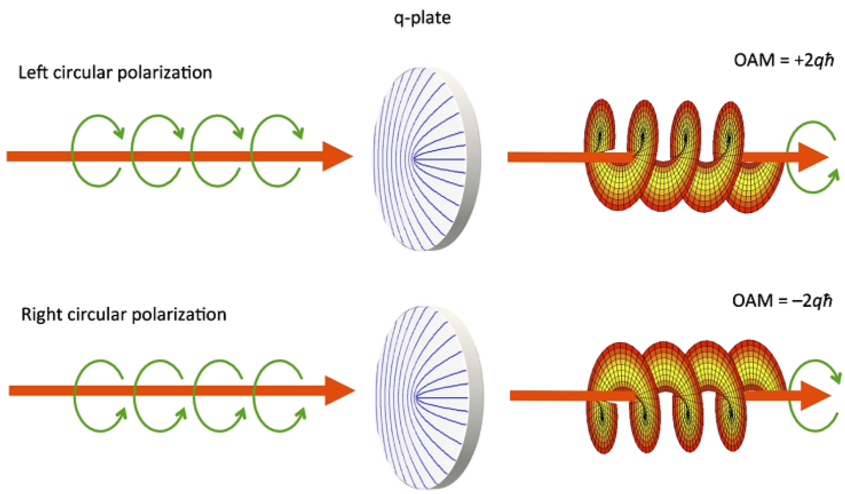

Figure 4.1: An illustration that shows how OAM modes can be imparted with a circularly polarized configuration using a q-plate.

Basically, a q-plate as illustrated in Figure 4.2 is a liquid crystal that has liquid crystal molecules embedded between two thin glass plates. this embedded material introduces the $q\phi$ parameter into the transformation of q-plates as depicted by equation 4.2. In general terms, with the aid of the q-plate, the states of polarization as represented in the Poincare sphere (A 3-dimensional spherical graphical tool showing different states of polarization of optical fields) can easily be transformed from one state to the other [Marrucci, (2013)].

The initial field passing through the q-plate has equal linear polarization as well as

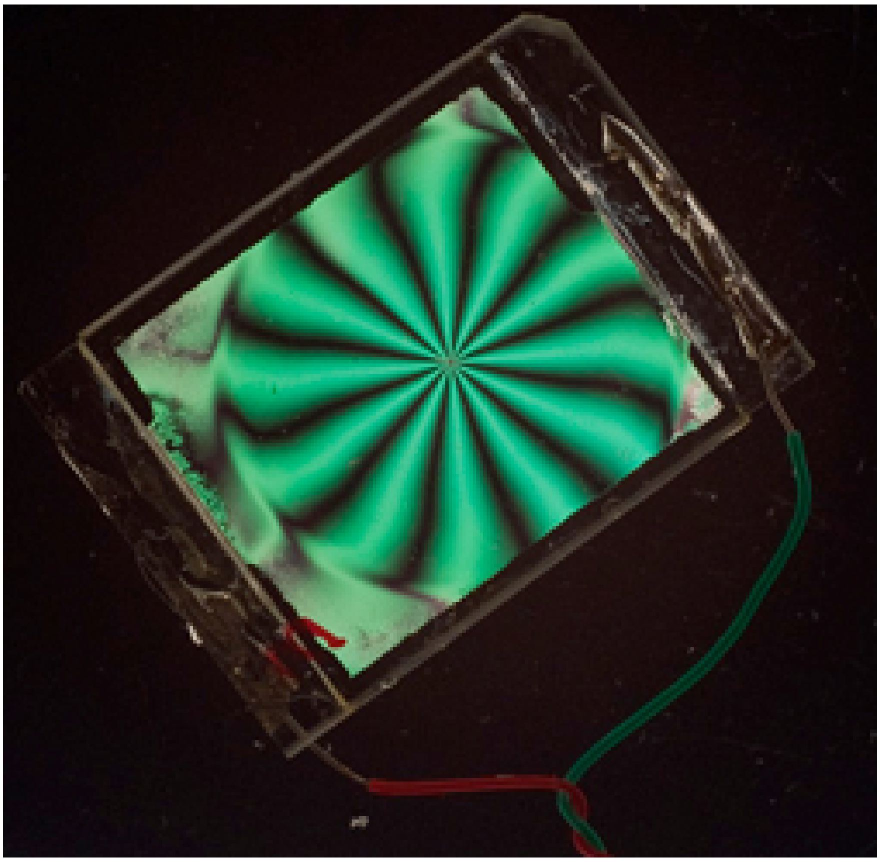

Figure 4.2: Description of a q-plate, the pattern is introduced as a result of the topological charge q.

equal weightings of left and right polarization. However, after the q-plate, the field becomes circularly polarized with right circularly polarized field decreasing in azimuthal topological charge of 1 and the left increasing with 1 thus leading to a superposition of a $l = 1$ and $l = -1$. The superposition can only be noticed when a polarizer is introduced thereby producing a petal-like beam [Dudley et al., 2013]. Example of the beams is shown in the experimental result section

Figure 4.3 is a table that illustrates the action of q-plates. With the inclusion of other optical elements (half wave plate), it is possible to manipulate the input beam of a particular OAM mode into another output field with a different vector or scalar mode.

Since the q-plates acts on the polarization of the optical field, it is easy to show the

Input polarization state	Action of q-plate	Output polarization state
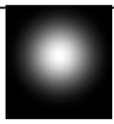 $\|0, L\rangle + \|0, R\rangle$	$q = 1/2$ $\|0, L\rangle \rightarrow \|0+1, R\rangle$ $\|0, R\rangle \rightarrow \|0-1, L\rangle$	 $\|-1, L\rangle + \|1, R\rangle$
 $\|-1, L\rangle + \|1, R\rangle$	q= $\frac{1}{2}$ with rule L $\rightarrow R$ and R $\rightarrow L$ $\|-1, L\rangle \longrightarrow \|1+1, R\rangle$ $\|1, R\rangle \rightarrow \|-1-1, L\rangle$	 $\|2, R\rangle +$ $\|-2, L\rangle$
 $\|-1, L\rangle + \|1, R\rangle$	q= $\frac{1}{2}$ with rule L $\rightarrow R$ and R $\rightarrow L$ $\|1, L\rangle \rightarrow$ $\|1-1, R\rangle$ $\|1-1, R\rangle \rightarrow \|-1+1, L\rangle$	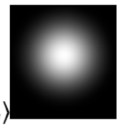 $\|0, R\rangle +$ $\|0, L\rangle$ $l = 0$
 $\|-2, L\rangle + \|2, R\rangle$	q= $\frac{1}{2}$ with rule L $\rightarrow R$ and R $\rightarrow L$ $\|-2, L\rangle \rightarrow$ $\|-2-1, R\rangle$ $\|2, R\rangle \rightarrow \|2+1, R\rangle$	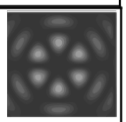 $\|3, R\rangle$ $+ \|-3, L\rangle$

Figure 4.3: Summary of the action of q-plate on different input beam with respective output beams, $\lambda = 1/2$ - half-wave plate.

procedure by considering a basis set of operation. In this case, dirac basis is used. Consider a Gaussian beam described by the basis element as:

$$|U\rangle = |0, R\rangle + |0, L\rangle \tag{4.1}$$

With the transformation introduced by a q-plate $q = \dfrac{1}{2}$ and having transformation rule given as:

$$|l, R\rangle \xrightarrow{q} |l - 2q, L\rangle\,, \quad |l, L\rangle \xrightarrow{q} |l + 2q, R\rangle \tag{4.2}$$

So that

$$|l, R\rangle \rightarrow |0 - 1, L\rangle \rightarrow |-1, L\rangle \tag{4.3}$$

$$|l, L\rangle \rightarrow |0 + 1, R\rangle \rightarrow |1, R\rangle \tag{4.4}$$

So that after the q-plate, the field becomes :

$$|1, R\rangle + |-1, L\rangle = \exp(i\phi)\begin{pmatrix} 1 \\ -i \end{pmatrix} + \exp(-i\phi)\begin{pmatrix} 1 \\ i \end{pmatrix} = \begin{pmatrix} \cos(\phi) \\ \sin(\phi) \end{pmatrix} \tag{4.5}$$

Where the two vector corresponds to the right and left circular polarization respectively.

4.2.1 Experimental setup for Vector Bessel beam generation

The experimental set up used for the generation of the beams is shown in Figure **??**. The setup comprises HeNe laser beam (633 nm), a spatial light modulator (SLM) (Holoeye, PLUTO-VIS with 1920 x 1080 pixel). The SLM is calibrated for a 2π phase shift at 633 nm). Other components includes a q-plate, aligning mirror, a polarizer, and a CCD camera. An aperture is inserted in-between the 4f system to filter out the zero and second diffraction order beams.

Firstly, a scalar Bessel beam was generated. This was done by propagating a Gaussian beam through an SLM and the output was captured by a CCD camera. A q-plate was introduced into the setup and the output beam gives a vector Bessel beam and thereafter a polarizer was inserted at several angles ranging between 0 and 2π with the output captured accordingly.

4.2.2 Results and Discussion for generated Vector Bessel beams

The captured results are shown in Figure 4.5. The recorded beam is a donut beam which indicates a singularity. This means, the beam carries an OAM that is yet to be verified. Next a polarizer was introduced to generate the various polarization state, these states are

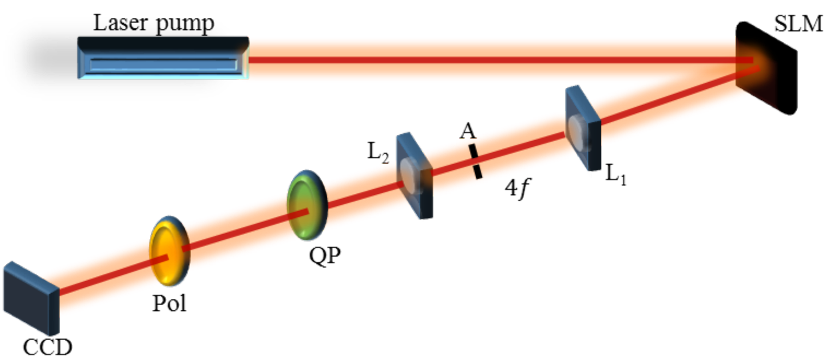

Figure 4.4: Experimental setup for the generation of Vector Bessel-Gaussian beam using digital axicons. M-mirror, SLM-spatial light modulator, Pol-polarizer, QP-q-plate, A-aperture, CCD-camera, Hene-Gaussian beam laser source.

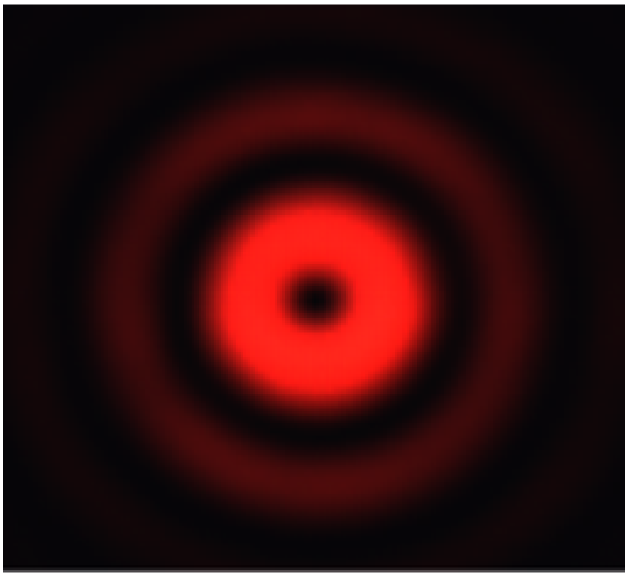

Figure 4.5: vector Bessel Gaussian beam for $l = 1$ and $l = -1$, the input beam was a $l = 0$.

horizontal, vertical, diagonal and anti-diagonal as illustrated in Figure 4.6.

The generated beams were classified into radial and azimuthal polarization as shown in Figure 4.7.

Next a half-wave plate was introduced alongside another q-plate to generate $|-2, L\rangle +$ $|2, R\rangle$ state with a $l = 0$ as the input state. With the correct combination of a q-plate and a half wave plate, it is possible to generate higher order of VBBs, however due to the myriad nature of the setup, the experiment was restricted to $|-2, L\rangle + |2, R\rangle$. Furthermore, a

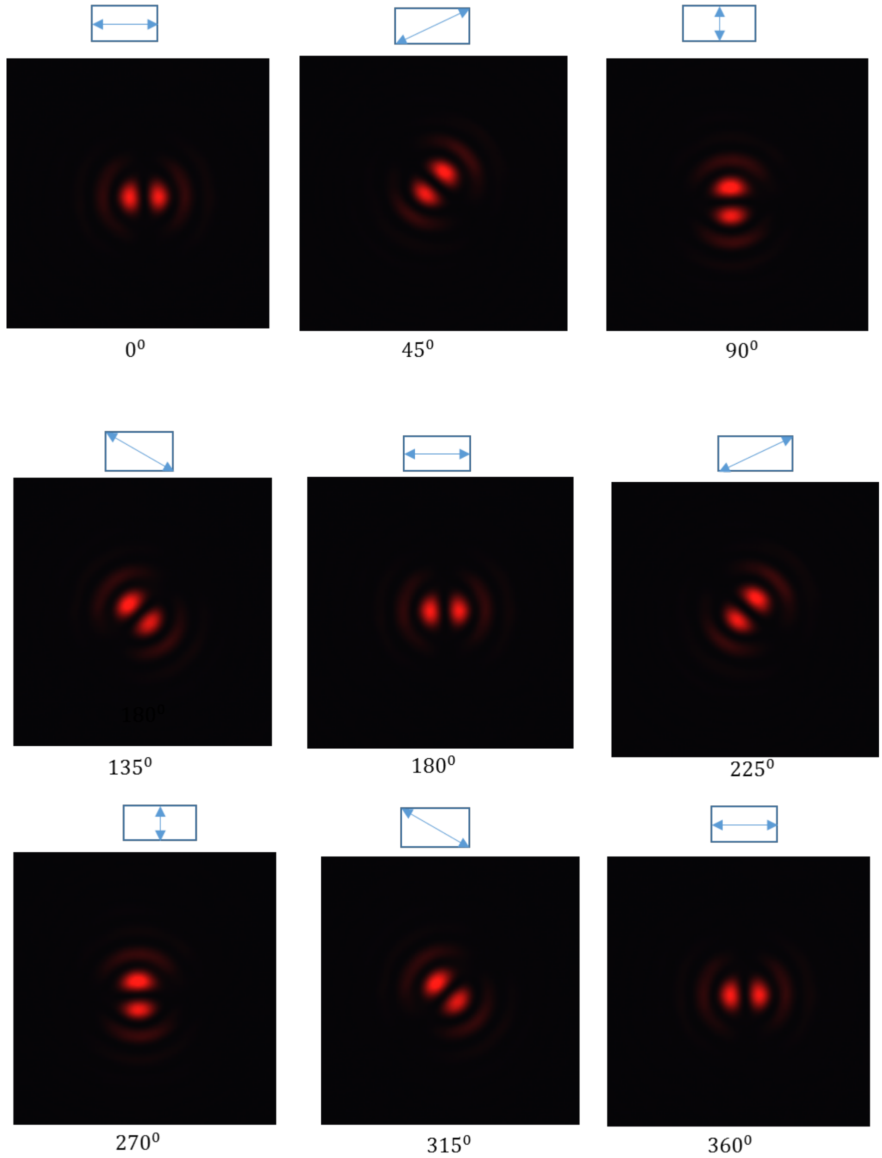

Figure 4.6: The various polarization state of the generated vector Bessel-Gaussian beams as captured by the CCD camera.

polarizer was introduced as in the case of $|-1, L\rangle + |1, R\rangle$ state to generate the different polarization state. Figure 4.9 is the captured polarization states, the polarizer was rotated between 0 and 2π.

In real sense, the generated vector Bessel beam is a superposition of $l = 1$ and $l = -1$ vector modes which have left and right circular polarization. Rotating the polarizer between 0 and 2π gives a varying polar angle of the beam leading to a radially polarized vector beam as shown in the first row of figure 4.7.

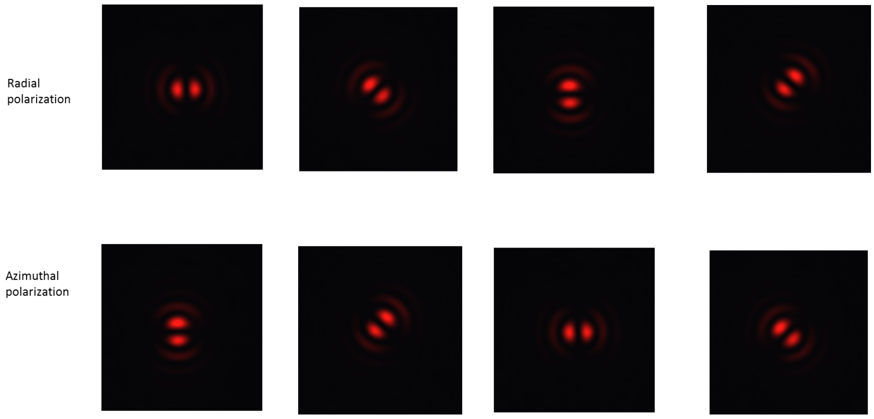

Figure 4.7: Classification of the vector Bessel-Gaussian beams into radial and azimuthal polarization.

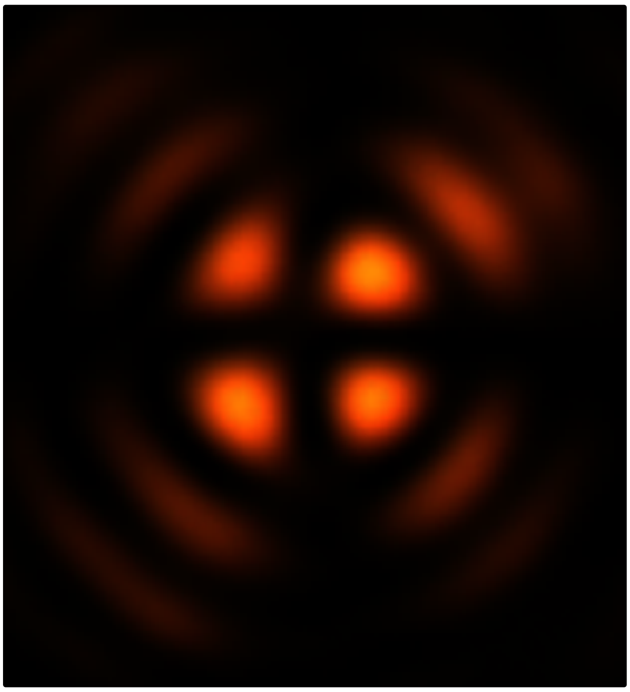

Figure 4.8: The captured intensity profile of $l = 2$ state with a Gaussian beam as the initial beam. Another half-wave plate and q-plate were included in the setup .

Similarly, when the polarizer is oriented at angle π, a phase offset is generated shifting the phase of the beam by a half period thereby leading to azimuthal polarization which is a tangential around the ring as described in cylindrical vector and vector fields beam section (section 2.5 and 2.4). This is shown in the second row of Figure 4.7. The same scheme can also be applied for higher order vector states. Both scenarios can be interchanged easily if the orientation angle is swapped around which means that the superposition of the

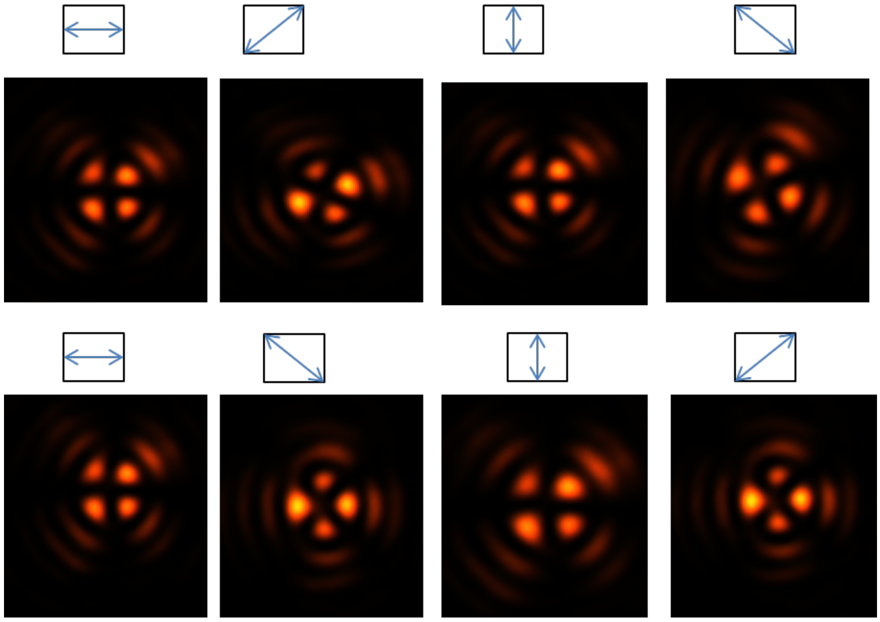

Figure 4.9: Different polarization state of the $|-2, L\rangle + |2, R\rangle$ vector Bessel-Gaussian beam defined by horizontal, diagonal, vertical and antidiagonal.

vector beams still gives a linear polarization due to the cylindrical symmetric nature of the beams.

4.3 Modal decomposition of Vector Bessel-Gaussian beams

In the case of vector Bessel beams, a quarter-wave plate was introduced. A quarter-wave plate (QWP) is an optical device that converts a circularly polarized beam to a linearly horizontal or vertically polarized beam depending on specific angles of the wave-plate. The action of the QWP on the vector Bessel beams is to decompose the coupled left and right circularly polarized beams into two independent scalar beams and the decomposition can be done separately on both beams. Conceptually,

$$\psi_l = \exp(il\psi) \tag{4.6}$$

with Jones matrix given as

$$\psi_l = \frac{1}{\sqrt{2}} \begin{pmatrix} 1 \\ i \end{pmatrix} \tag{4.7}$$

and the QWP denoted by L_{45} with Jones matrix

$$L \pm 45 = \frac{1}{\sqrt{2}} \begin{pmatrix} 1 & \pm i \\ \pm i & 1 \end{pmatrix} \tag{4.8}$$

so that

$$L_{+45} |1, H\rangle = \frac{1}{\sqrt{2}} \begin{pmatrix} 1 & \pm i \\ \pm i & 1 \end{pmatrix} \begin{pmatrix} \psi_1 \\ i \end{pmatrix} \tag{4.9}$$

which after some algebraic manipulations gives

$$L_{-45} |1, H\rangle = \frac{1}{\sqrt{2}} \psi_l C_+ = |-1, L\rangle \tag{4.10}$$

Similarly for ψ_{-1}

$$\psi_{-1} = \exp(-il\psi) = L_{+45} |1, H\rangle = \frac{1}{\sqrt{2}} \psi_l C_- = |1, R\rangle \tag{4.11}$$

Equation 4.10 and 4.11 indicates the two independent left and right sided states. With the aid of the quarter wave plate, modal decomposition can be implemented on both states independently.

The setup for the modal decomposition is shown in Figure 4.10). The setup for the modal decomposition is similar to the scalar case, the difference is that , in the case of the scalar Bessel beams, the q-plate and QWP were excluded. Here, the SLM is partitioned into

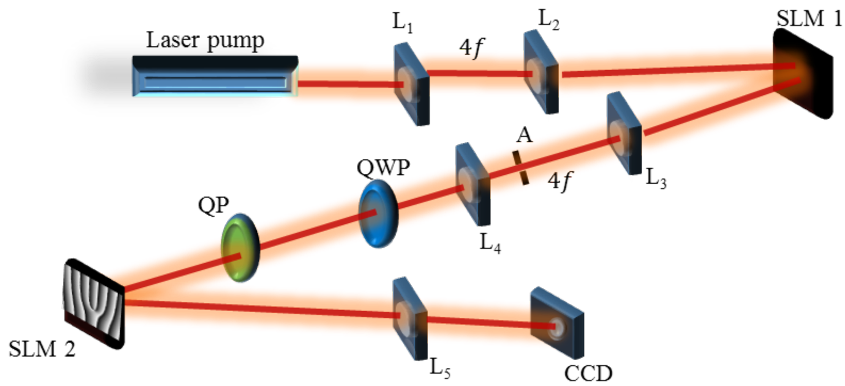

Figure 4.10: Setup for modal decomposition of the vector Bessel beams $L1 = 200$ mm, $L2 = 200$ mm, $L3 = 100$ mm, $L4 = 100$ mm, $L5 = 300$ mm, QWP-quarter wave plate, pol-polarizer,q-qplate, A-aperture used to seperate first diffraction order, SLM-spatial light modulator, CCD-camera.

two, one part for generating the Bessel beams and the other for the modal decomposition. The first $4f$ system was to image the Bessel beam plane into another plane so that the second $4f$ system images the beam back into the second part of the SLM. The first SLM was encoded with the transfer function of an Axicon with an extra helical phase, the second SLM was encoded with the same function but with an opposite sign of phase. $L5$ was the Fourier lens used for the inner product generation for the second SLM.

Firstly, the inner product measurement was also performed for the Bessel beam without the QWP. Measurements were taken for topological l values rannging from 5 to -5. $L \pm 45$ scheme was implemented by rotating the QWP between -45^0 and $+45^0$ concurrently. Here, L is the Jones matrix operator describing the action of the Quarter wave plate on the super positioned state. The procedure was repeated for the values ranging between $l = -5$ and $l = 5$.

4.3.1 Results for modal decomposition

The intensity plot of the detected vector BG is shown in Figure 4.11. the results are similar to that of the scalar BG beams. Only input modes matching the implemented filter gives a bright on-axis intensity. This is represented by the high peak in the graph otherwise a zero intensity is observed. This is the zero mark shown in the graph. It can also observed that -45^0 rotations of the quarter wave plate corresponds to $l = 1$ as in the case of scalar Bessel beams as well as 45^0 rotation corresponds to $l = 1$. This is in agreement with that obtained in the scalar Bessel beams.

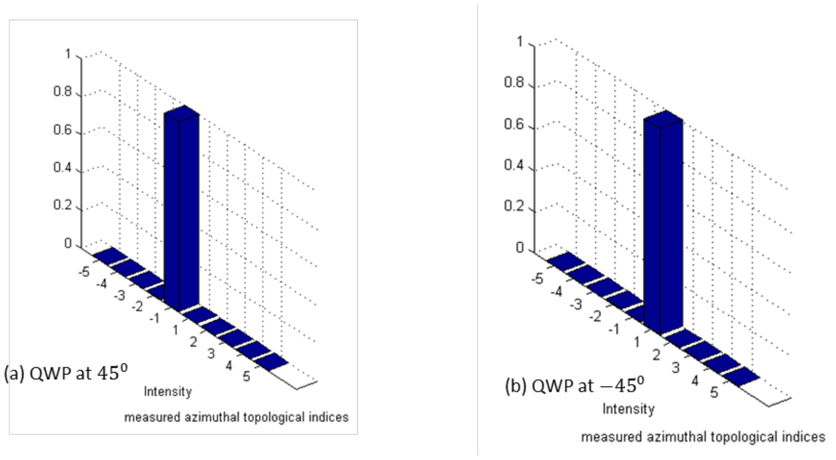

Figure 4.11: Detection of Vector Bessel-Gaussian beams using a Quarter wave plate set at -45^0 and 45^0.

4.4 Measurement of Vectorness of Bessel beams

Polarization involves electric field propagating in a single direction. Spatial polarization on the other hand comprrises vertical and horizontal polarization. One basic feature of vector beams is the coupling of polarization and spatial mode profile of the field. This coupling describes vectorness of light beams i.e it is the degree of non-separability (a beam with varying polarization over a traverse plane) of vector modes [McLaren et al., 2015].

The coupling in a vector beams can be visualized as an entanglement of a quantum system.The information contained in an entangled state has a dependence on its Hilbert space (abstract vector space having the structure of an inner product allowing length and angle measurement). The spatial mode profile of a photon contains an infinite number of dimensions of Hilbert space. This implies that the quantum information carrying capacity of photons is dependent on the degree of entanglement of optical fields [McLaren et al., (2014)]. Vector Bessel beams possess this coupling nature and there is a need to explore the possibility of measuring this non-separability nature of these beams. Consider an electric field paraxial vector describing a light beam given as:

$$E(t) = E_0 e^{(iwt)} \Psi(t) \tag{4.12}$$

where the propagation is along the z-direction and w is the frequency. The unit vector field with complex unit-amplitude can be written as:

$$\Psi(r, \phi, z) = \sqrt{a} U_R(r, \phi, z) \boldsymbol{e_R} + \sqrt{(1-a)} U_L(r, \phi, z) \boldsymbol{e}_L \tag{4.13}$$

Here, $'a'$ is the relative weighting of the fields U_R and U_L. Equation 4.13 can be re-written in the bra-ket format as:

$$|\Psi\rangle = \sqrt{a}\, |U_R\rangle \otimes |R\rangle + \sqrt{(1-a)}\, |U_L\rangle \otimes |L\rangle \tag{4.14}$$

$|U_R\rangle$ and $|U_L\rangle$ are unit vectors in the Hilbert space describing the complex spatial field in transversal plane. $\otimes$ symbol is the tensor product between the vectors and it enables the description of the entangled state [McLaren, (2014)]. Now consider the case where $a = \dfrac{1}{2}$

and assuming the two modes $|U_R\rangle$ and $|U_L\rangle$ are orthogonal, it leads to a maximally entangled state and in turn gives a pure vector field however in the case where $a = 1$ or 0, both modes are the same and thus yields a scalar field. The amount of information contained in the photon is much dependent on the basis in which the measurement of the quantum state is done. For instance, a qubit system carries only two bits of information per photon whereas a qudit system carries d bits of information [McLaren t al., (2012)].

4.4.1 Quantum Tomography with application to vectorness measurement of Vector Bessel-Gaussian beams.

Quantum tomography involves the characterization of a quantum system using a set of identical particles. The process reconstructs a quantum state from series of eigenbases. The procedure can be visualized as scanning a 3-dimensional object from different angles [Altepeter et al., (2005)]. In terms of measurement of vectorness (described in the previous section), the tomography tool can be used to measure the vectorness of the generated vector Bessel beams. The tool measures the coupling of the various polarization states with the corresponding spatial input modes (OAMs) [Ndagano et al., (2015)]. The procedural implementation involves using two SLMs which in this case, The SLM was partitioned into two. The OAMs in the form of holograms was encoded into SLM2 and the correlation filter as obtainable in the case of modal decomposition is encoded into SLM1. Modal decomposition is simultaneously performed for each of the polarization states as an on-axis intensity is measured in each of the cases.

4.5 Experimental setup for measure of vectorness

The experimental setup is similar to that of modal decomposition both for scalar and vector case of the Bessel beam and is illustrated in Figure **??**, the addition in this case is

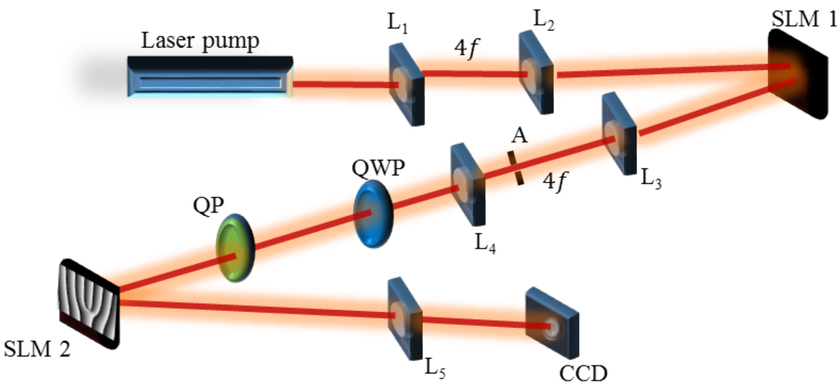

Figure 4.12: Setup for the measure of vectorness of the vector Bessel beams using quantum tomography $L1 = 200$ mm, $L2 = 200$ mm, $L3 = 100$ mm, $L4 = 100$ mm, $L5 = 300$ mm, QWP-quarter wave plate, pol-polarizer,q-qplate, A-aperture used to seperate first diffraction order, SLM-spatial light modulator, CCD-camera.

the inclusion of a half wave plate (HWP) for the measurement of the polarization state (horizontal, vertical, diagonal and anti-diagonal) and a quarter wave plate (right and left circularly polarization state). These optical devices (HWP and QWP) are inserted before SLM2. The OAMs encoded on SLM2 consist of the superposition of $|l = 1\rangle + \exp(i\theta_2)\,|l = -1\rangle$ for the first two holograms and the other four are the different orientations for $\theta_2 = 0$, $\pi/2$, π and $3\pi/2$. In the second case of vector Bessel beams, a q-plate is introduced at position $\frac{1}{2}Z_{max}$ to convert the scalar BG beams to vector BG beams before the quarter and half wave plates are consequently introduced to select the corresponding polarization state. The position of the quarter-wave plate is oriented at $\pm\pi/4rad$ and the half-wave plate oriented between the angles 0^0 and subsequently at 22.5^0 for other polarization state measurement.

The tomography arrangement generates 36 measurements in the form of a 6X6 matrix. The measurement can thus be used to reconstruct the density matrix $\rho = |\Psi\rangle\langle\Psi|$

and the vectorness can be calculated using the density matrix.

4.5.1 Results and Discussion for measure of vectorness

The 6×6 matrix generated from the tomography procedure for both scalar and vector BG respectively are shown in Figure 4.13 as well the vector case It was observed that

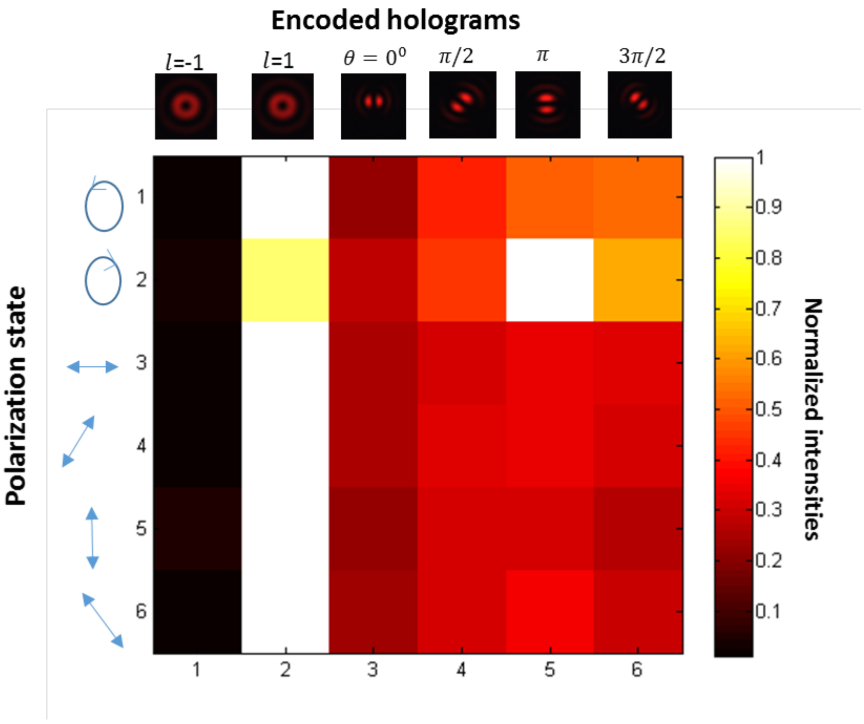

Figure 4.13: Tomography generated matrix for scalar Bessel-Gaussian beams which describes the coupling between polarization state and the corresponding OAMs.

in the case of the Scalar BG beams as illustrated in Figure 4.13, that for $l = -1$, it is all zeros, this is due to the fact that there is no coupling between the OAM $l = 1$ and $l = -1$ and there can only be one OAM mode which is $l = 1$ having all $1s$ and no such mode as $l = -1$. This is different in the case of Vector BG beam as illustrated in Figure 4.14). Since there is a coupling of the state $|1, L\rangle + |-1, R\rangle$ such that for the coupling of left and right circular polarization with $l = 1$ and $l = -1$ OAM, an on-axis intensity and no-axis intensity was observed in both cases, this is due to the correlation filter matching of the input modes and the detecting modes.

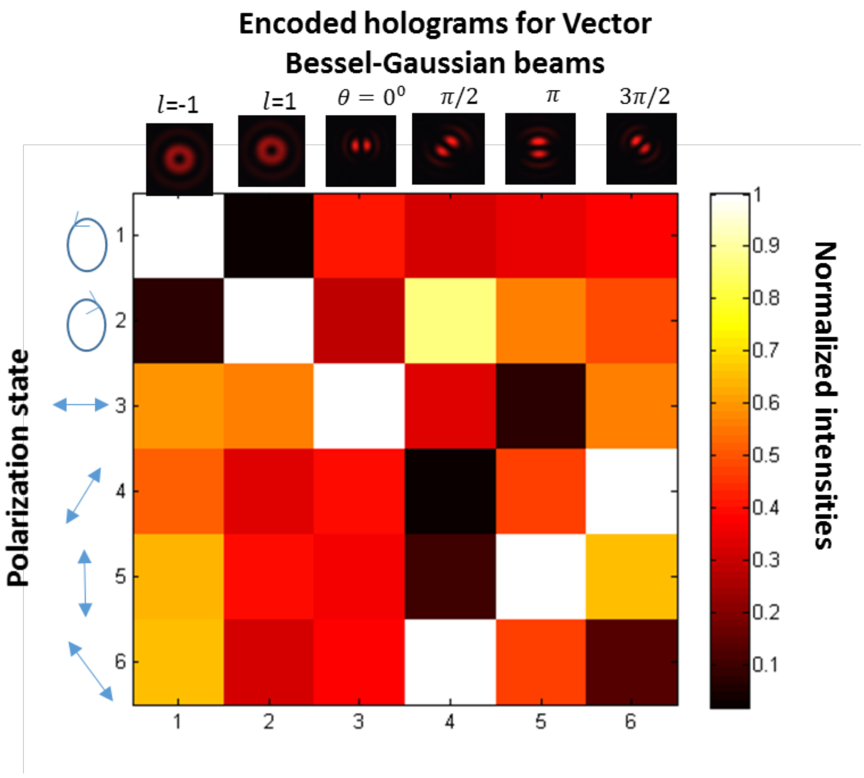

Figure 4.14: Experimentally measured tomographic matrix describing the coupling the 6 polarization state with the corresponding input OAMs for vector BG beams.

For the other inner product between the OAMs and polarization state leading to $\frac{1}{2}$ intensity, it can be seen mathematically as:

$$\langle 1, H| \left(|1, H\rangle + |1, V\rangle\right) = \frac{1}{\sqrt{2}} \langle H|H\rangle \tag{4.15}$$

So that the square of the absolute value yields a $\frac{1}{2}$, the value is almost the same for the others as it is just a change of orientation of the holograms. However, in the vector case where there is a zero intensity, this is due to the orientation becoming orthogonal in terms of the coupling of the polarization state and OAM mode and thus gives a zero. The density matrix for the scalar Bessel beam is shown below in Figure 4.15. The concurrence which is the measure of the degree of non-separability is $C = 0.05 \pm 0.01$ and fidelity which is the measure of the how close the non-separability of the quantum states are is $F = 0.06 \pm 0.01$. This is a clear indication that the states in a scalar Bessel beam are not entangled or separable. this is due

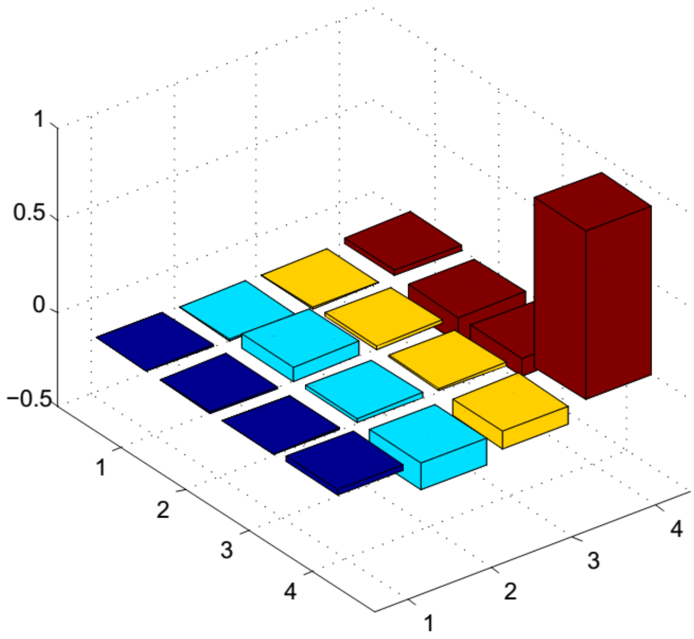

Figure 4.15: Density matrix describing the inner product $\rho = |\psi\rangle\langle\psi|$ of scalar Bessel-Gaussian beams.

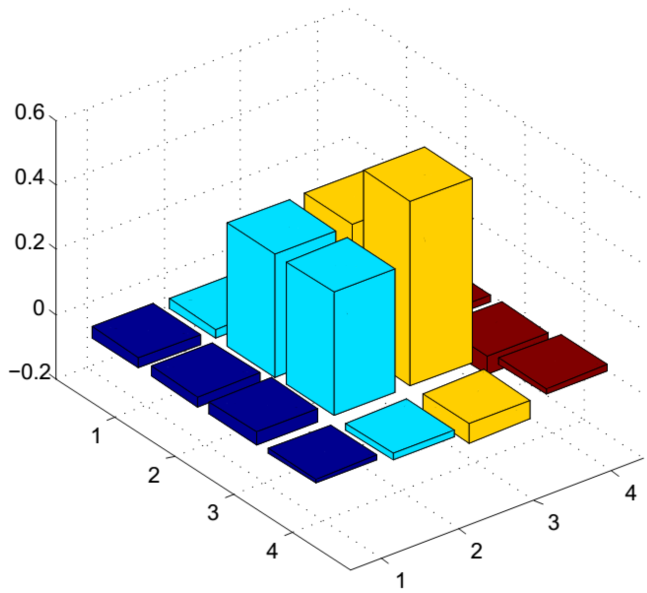

Figure 4.16: Density matrix representation of vector Bessel beams describing the coupling of $l = 1$ and $l = -1$ OAM modes.

to the fact that there is no coupling between -1 and 1 OAM mode. it was observed that in the density matrix a region of high intensity, this correlates with the earlier result in the tomographic representation with the on-axis intensity in the case of $l = 1$. Only one state is represented at a time which is the $l = 1$ OAM mode.

The density matrix of vector case is shown in Figure 4.16). The concurrence and fidelity are $C = 0.76 \pm 0.01$ and $F = 0.86 \pm 0.01$ respectively. These are obvious indication that the coupled modes preserve non-separability tendencies and the closeness (fidelity) to non-separability is adequate to describe the coupled state of the vector beam.
These measurements show an indication that the generated vector beam is good enough for relevant application such as optical trapping and microscopy e.t.c.

4.6 Summary

Q-plates are birefringent optical devices that enables the coupling of spatial modes of OAM and polarization states was introduced in this section, Quantum tomography as a tool for measuring vectorness was also presented. Experiments for generation and detection of Vector BBs were presented in this section as well. Due to the coupling of the -1 and $+1$ OAM mode, a quarter wave plate is used to decompose the coupled mode into two independent modes and modal decomposition implemented on both modes seperately. The obtained result in the case of the detection is similar to the case of scalar Bessel beams as expected. The obtained result in the vectorness measurement also indicates that the states in the vector modes are entangled which is in correlation to theory as expected.

Chapter 5

Conclusion and Future work

5.1 Introduction

The results obtained in this research work are presented in this section. Generation and detection of scalar beams were firstly presented. This is followed by generation and detection of vector Bessel beams and finally the measure of vectorness are presented.

5.2 Conclusion

This research work was focused on generating and detecting vector Bessel beams. Firstly scalar beams were generated using the phase of an Axicon. The scalar Bessel beams were generated at propagating distance $\approx$ 14 cm using an Axicon angle of 0.2^0 with a beam waist of 0.5 mm. The obtained zero order beam was a bright spot on-axis intensity beam. The higher order Bessel beams was a donut beam with a dark spot which depicts the vorticity of the beam. A polarizer was used to analyze the polarization state of the scalar beams and it was observed that the spatial position of the beams remain unchanged which indicates the partial nature of the scalar beams. Using a two partitioned spatial light modulator, modal decomposition was implemented on the scalar beams. When the input OAM of $l = 1$ matches the correlation filter that was encoded on the other part of the SLM, a bright on-axis intensity was captured at the CCD camera. In the case where there is a mismatch, a null on-axis was captured by the CCD.

In terms of vector Bessel beam generation, a q-plate was introduced at the point where the scalar beams were formed. The vector beams is a donut beam like that of the higher order scalar Bessel beam with a coupling of $|-1, L\rangle + |1, R\rangle$ OAM modes. A $|-2, L\rangle + |2, R\rangle$ vector Bessel beam was also generated with the introduction of another q-plate and a half wave plate. Regarding the detection of the vector Bessel beams, a quarter wave plate tuned at $\pm 45^0$ was used to decompose the coupled beam into two independent linearly polarized beams and the modal decomposition performed on both beams seperately. The obtained results are similar to that of the scalar beams such that $l = 1$ mode corresponds to 45^0 and $l = -1$ OAM modes correlates with -45^0 angle orientation of the quarter wave plate.

Finally, The measure of vectorness was explored using quantum tomography tool. The density matrix was reconstructed from the measurement obtained from the state tomography. The density matrix is used to calculate the concurrence and Fidelity. The value of concurrence which is the measure of non-separability of the vector modes and fidelity which is the measure of the closeness of the non-separability were found to be $C = 0.76 \pm 0.01$ and $F = 0.86 \pm 0.01$.

Most researches that have been done on generation of vector Bessel beams was by annular slits. The digital Axicon and q-plate technique implemented in this research also provide an effective way of generating vector Bessel beams. The measure of vectorness was an extension of the research in comparison with other research that has been done in the area of vector Bessel beams.

5.3 Future Work

Concerning future research work, application of the generated Bessel-Gaussian beams particularly to optical trapping of microbial particles a would be considered. Brief concept of the application of vector Bessel beams to trapping is described in the next section.

5.3.1 Application of vector Bessel beams to optical turbulence

Optical turbulence (OT) is one area that has received significant attention recently. vector beams are assumed to fare better in atmospheric turbulence.

5.3.2 Problem statement

The atmosphere which naturally contains moisture and temperature gradients leads to turbulent motion. The effect of this motion creates disturbances in the atmosphere's refractive index. Optical turbulence (OT) on the other hand is described by the atmospheric refractive index in the form of cells usually referred to as optical tubules. OT occurs as a result of the fluctuation in the refractive index from temperature changes. Slight stochastic variation of atmospheric refractive can lead to an observable effect on the optical wave in terms of intensity and phase aberrations [Hagelin, Susanna, et al., (2008)].

Although, these distortions may be very small in size but its cumulative effect is enormous after long distance propagation. Generally, as the altitude increases in the atmosphere, the result is a decrease in temperature and less pressure on the mass of air which affects the expansion of the air. The situation reverses when the height of the atmosphere decreases. With the motion of air mass or wind in the atmosphere, there is a significant increase in turbulence due to temperature fluctuations and the effect can be compounded if there is increased the friction of air mass [Juarez, C., David M. and David W., (2013)]. Understanding how beams behave when propagating through turbulence gives an insight into the behaviour of waves during free space and wireless communications and possibly understand how the inefficiencies can be managed. A couple of studies that have been done in this area involves simulations and not actual experimental procedure [Chen, B., Chen, Z. and Pu, J., (2008), Eyyuboğlu, H. T., (2007), Qin, Zhiyuan, et al., (2014)]. The proposed study adopts a simple experimental approach.

5.3.3 Background

Consider a propagating Gaussian beam with waist w_0, the introduction of the variable refractive index along the path of the beam causes abnormalities such as wave front deflections and lensing effects (bending of light passing through the lens). The effects might seem very insignificant but cumulatively causes enormous wave-vector spreading of the beam [Gopaul, C., and R. Andrews, (2007)].

Furthermore, considering the Fried parameter and its relationship with the beam waist which is expressed as

$$\frac{w_0}{r_0} = \frac{(w_{le}/w_{dl}) - 1}{3.0} \tag{5.1}$$

Where w_{le} and $w_d l$ are the non-diffractive and long-exposure of the far-field radius of the broadened optical field. The Fried parameter r_0 is given as

$$r_0 = 3.02(k^2 L C_n^2)^{-3/5} \tag{5.2}$$

With k been the usual wave-vector number of wavelength given as $k = \dfrac{2\pi}{\lambda}$, L is the propagation length and C_n^2 been the refractive index structure constant which describes the strength of the refractive index anomalies. Usual values of the structure constant ranges between 10^{17} to 10^{14} $\mathrm{m}^{2/3}$ for mild conditions and strong turbulent conditions respectively. The constant parameter is high within a short distance above sea level and drops quickly as height increases [Andrews, L. and Phillips, R., (2005)].

Bibliography

[Altepeter et al., (2005)] Altepeter, J.B., Jeffrey, E.R. and Kwiat, P.G., 2005. Photonic state tomography. Advances in Atomic, Molecular, and Optical Physics, 52, pp.105-159.

[Ambs et al., (2007)] Ambs, P., Otón, J., Millán, M.S., Jaulin, A. and Bigué, L., 2007, June. Spatial light modulators for information processing: applications and overview. In AIP Conference Proceedings (Vol. 949, p. 226). IOP INSTITUTE OF PHYSICS PUBLISHING LTD.

[Andrews, L. and Phillips, R., (2005)] Andrews, L.C. and Phillips, R.L., 2005. Laser beam propagation through random media (Vol. 52). Bellingham, WA: SPIE press.

[Arlt, J., and K. Dholakia, (2000)] Arlt, J. and Dholakia, K., 2000. Generation of high-order Bessel beams by use of an axicon. Optics Communications, 177(1), pp.297-301.

[Arlt et al, 2001] Arlt, J., Garces-Chavez, V., Sibbett, W. and Dholakia, K., 2001. Optical micromanipulation using a Bessel light beam. Optics Communications, 197(4), pp.239-245.

[Ashkin et al., (1987)] Ashkin, A., Dziedzic, J.M. and Yamane, T., 1987. Optical trapping and manipulation of single cells using infrared laser beams. Nature, 330(6150), pp.769-771.

[Basistiy et al., (1995)] Basistiy, I.V., Soskin, M.S. and Vasnetsov, M.V., 1995. Optical wavefront dislocations and their properties. Optics Communications, 119(5), pp.604-612.

[Beresna et al., (2015)] Beresna, M., Gecevičius, M. and Kazansky, P.G., 2015. Harnessing Ultrafast Laser Induced Nanostructures in Transparent Materials. In Progress in Nonlinear Nano-Optics (pp. 31-46). Springer International Publishing.

[Berkhout G. and Marco W., (2010)] Berkhout, G.C. and Beijersbergen, M.W., 2010. Measuring optical vortices in a speckle pattern using a multi-pinhole interferometer. Optics express, 18(13), pp.13836-13841.

[Birch et al., (2000)] Birch, P.M., Young, R., Budgett, D. and Chatwin, C., 2000. Two-pixel computer-generated hologram with a zero-twist nematic liquid-crystal spatial light modulator. Optics letters, 25(14), pp.1013-1015.

[Bouchal et al., (1998)] Bouchal, Z., Wagner, J. and Chlup, M., 1998. Self-reconstruction of a distorted nondiffracting beam. Optics Communications, 151(4), pp.207-211.

[Bouchal, 2003] Bouchal, Z., 2003. Nondiffracting optical beams: physical properties, experiments, and applications. Czechoslovak journal of physics, 53(7), pp.537-578.

[Bouchal and Celechovský, (2004)] Bouchal, Z. and Celechovský, R., 2004. Mixed vortex states of light as information carriers. New Journal of Physics, 6(1), p.131.

[Burvall et al., (2005)] Burvall, A., Goncharov, A. and Dainty, C., 2005. Telephoto axicon. In Optical Systems Design 2005 (pp. 596213-596213). International Society for Optics and Photonics.

[Cardano et al., (2012)] Cardano, F., Karimi, E., Slussarenko, S., Marrucci, L., de Lisio, C. and Santamato, E., 2012. Polarization pattern of vector vortex beams generated by q-plates with different topological charges. Applied optics, 51(10), pp.C1-C6.

[Chattrapiban et al., (2003)] Chattrapiban, N., Rogers, E.A., Cofield, D., Hill III, W.T. and Roy, R., 2003. Generation of nondiffracting Bessel beams by use of a spatial light modulator. Optics letters, 28(22), pp.2183-2185.

[Chávez-Cerda, (1999)] Chávez-Cerda, S., 1999. A new approach to Bessel beams. Journal of modern optics, 46(6), pp.923-930.

[Chen, B., Chen, Z. and Pu, J., (2008)] Chen, B., Chen, Z. and Pu, J., 2008. Propagation of partially coherent Bessel-Gaussian beams in turbulent atmosphere. Optics and Laser Technology, 40(6), pp.820-827.

[Dudley et al., (2012)] Dudley, A. and Forbes, A., 2012. From stationary annular rings to rotating Bessel beams. JOSA A, 29(4), pp.567-573.

[Dudley et al., (2013)] Dudley, A., Li, Y., Mhlanga, T., Escuti, M. and Forbes, A., 2013. Generating and measuring nondiffracting vector Bessel beams. Optics letters, 38(17), pp.3429-3432.

[Dudley et al., 2013] Dudley, A., Mhlanga, T., McDonald, A., Roux, F.S., Lavery, M., Padgett, M. and Forbes, A., 2013, September. Techniques to sort Bessel beams. In SPIE Optical Engineering+ Applications (pp. 884306-884306). International Society for Optics and Photonics.

[Duocastella and Arnold, (2012)] Duocastella, M. and Arnold, C.B., 2012. Bessel and annular beams for materials processing. Laser and Photonics Reviews, 6(5), pp.607-621.

[Durnin et al., (1987)] Durnin, J., Miceli Jr, J.J. and Eberly, J.H., 1987. Diffraction-free beams. Physical Review Letters, 58(15), p.1499.

[Durnin et al., (1987)] Durnin, J., 1987. Exact solutions for nondiffracting beams. I. The scalar theory. JOSA A, 4(4), pp.651-654.

[Erikson and Singh, (1994)] Erikson, W.L. and Singh, S., 1994. Polarization properties of Maxwell-Gaussian laser beams. Physical Review E, 49(6), p.5778.

[Eyyuboğlu, H. T., (2007)] Eyyuboğlu, H.T., 2007. Propagation of higher order Bessel–Gaussian beams in turbulence. Applied Physics B, 88(2), pp.259-265.

[Ferreira and Belsley, (2010)] Ferreira, F.P. and Belsley, M.S., 2010. Direct calibration of a spatial light modulator by lateral shearing interferometry. Optics express, 18(8), pp.7899-7904.

[Forbes, (2014)] Forbes, A. ed., 2014. Laser beam propagation: generation and propagation of customized light. CRC Press.

[Griffiths and Reed, (1999)] Griffiths, D.J. and Reed College, 1999. Introduction to electrodynamics (Vol. 3). Upper Saddle River, NJ: prentice Hall.

[Garcés-Chávez, V. et al, (2003)] Garcés-Chávez, V., McGloin, D., Padgett, M.J., Dultz, W., Schmitzer, H. and Dholakia, K., 2003. Observation of the transfer of the local angular momentum density of a multiringed light beam to an optically trapped particle. Physical review letters, 91(9), p.093602.

[Gopaul, C., and R. Andrews, (2007)] Gopaul, C. and Andrews, R., 2007. The effect of atmospheric turbulence on entangled orbital angular momentum states. New Journal of Physics, 9(4), p.94.

[Guo, Hanming, et al., (2011)] Guo, H., Weng, X., Dong, X., Sui, G., Gao, X. and Zhuang, S., 2011. Three dimensional optical cage formed by TEM01 mode radially polarized Laguerre-Gaussian beam. Journal of Optics, 40(4), pp.206-212.

[Guo-qin et al., (1996)] Guo-qing, Z., Bi-zhen, D., Guo-zhen, Y. and Ben-yuan, G., 1996. Design of diffractive-phase axicon illuminated by a Gaussian-profile beam. Acta Physica Sinica (Overseas Edition), 5(5), p.354.

[Hagelin, Susanna, et al., (2008)] Hagelin, S., Masciadri, E., Lascaux, F. and Stoesz, J., 2008. Comparison of the atmosphere above the South Pole, Dome C and Dome A: first attempt. Monthly Notices of the Royal Astronomical Society, 387(4), pp.1499-1510.

[Ismail et al., (2012)] Ismail, Y., Khilo, N., Belyi, V. and Forbes, A., 2012. Shape invariant higher-order Bessel-like beams carrying orbital angular momentum. Journal of Optics, 14(8), p.085703.

[Ito et al., (2010)] Ito, A., Kozawa, Y. and Sato, S., 2010, January. Generation of Cylindrical Vector Beams of a Single Higher Order Transverse Mode. In Advanced Solid-State Photonics (p. AMB20). Optical Society of America.

[Iizuka, (2002)] Iizuka, K., 2002. Elements of Photonics, In Free Space and Special Media (Vol. 1). John Wiley and Sons.

[Juarez, C., David M. and David W., (2013)] Juarez, J.C., Brown, D.M. and Young, D.W., 2013, May. Strehl ratio simulation results under strong turbulence conditions for actively compensated free-space optical communication systems. In SPIE Defense, Security, and Sensing (pp. 873207-873207). International Society for Optics and Photonics.

[Kaiser, T., Schröter, S. and Duparré, M, (2009)] Kaiser, T., Schröter, S. and Duparré, M., 2009. Modal decomposition in step-index fibers by optical correlation analysis. In SPIE LASE: Lasers and Applications in Science and Engineering (pp. 719407-719407). International Society for Optics and Photonics.

[Kaiser et al., (2009)] Kaiser, T., Flamm, D., Schröter, S. and Duparré, M., 2009. Complete modal decomposition for optical fibers using CGH-based correlation filters. Optics express, 17(11), pp.9347-9356.

[Kohno, M. and Matsuoka, Y., 2004] Kohno, M. and Matsuoka, Y., 2004. Microfabrication and drilling using diffraction-free pulsed laser beam generated with axicon lens. JSME International Journal Series B Fluids and Thermal Engineering, 47(3), pp.497-500.

[Kuo et al., (1993)] Kuo, S.C. and Sheetz, M.P., 1993. Force of single kinesin molecules measured with optical tweezers. Science, 260(5105), pp.232-234.

[Kwok et al., (2013)] Kwok, H.S., Naemura, S. and Ong, H.L. eds., 2013. Progress in Liquid Crystal Science and Technology: In Honor of Shunsuke Kobayashi's 80th Birthday (Vol. 4). World Scientific.

[Lai, W. et al., (2008)] Lai, W.J., Lim, B.C., Phua, P.B., Tiaw, K.S., Teo, H.H. and Hong, M.H., 2008. Generation of radially polarized beam with a segmented spiral varying retarder. Optics express, 16(20), pp.15694-15699.

[Lazarev, Grigory, et al,(2012)] Lazarev, G., Hermerschmidt, A., Krüger, S. and Osten, S., 2012. LCOS spatial light modulators: trends and applications. Optical Imaging and Metrology: Advanced Technologies, pp.1-30.

[Leach et al., (2006)] Leach, J., Gibson, G.M., Padgett, M.J., Esposito, E., McConnell, G., Wright, A.J. and Girkin, J.M., 2006. Generation of achromatic Bessel beams using a compensated spatial light modulator. Optics express, 14(12), pp.5581-5587.

[Litvin et al., (2015)] Litvin, I.A., Mhlanga, T. and Forbes, A., 2015. Digital generation of shape-invariant Bessel-like beams. Optics express, 23(6), pp.7312-7319.

[López-Mariscal and Gutiérrez-Vega, (2007)] López-Mariscal, C. and Gutiérrez-Vega, J.C., 2007. The generation of nondiffracting beams using inexpensive computer-generated holograms. American Journal of Physics, 75(1), pp.36-42.

[Marrucci et al., (2006)] Marrucci, L., Manzo, C. and Paparo, D., 2006. Optical spin-to-orbital angular momentum conversion in inhomogeneous anisotropic media. Physical review letters, 96(16), p.163905.

[Marrucci et al., (2011)] Marrucci, L., Karimi, E., Slussarenko, S., Piccirillo, B., Santamato, E., Nagali, E. and Sciarrino, F., 2011. Spin-to-orbital conversion of the angular momentum of light and its classical and quantum applications. Journal of Optics, 13(6), p.064001.

[Marrucci, (2013)] Marrucci, L., 2013. The q-plate and its future. Journal of Nanophotonics, 7(1), pp.078598-078598.

[Martínez-León et al., (2009)] Martínez-León, L., Jaroszewicz, Z., Kołodziejczyk, A., Durán, V., Tajahuerce, E. and Lancis, J., 2009. Phase calibration of spatial light modulators by means of Fresnel images. Journal of Optics A: Pure and Applied Optics, 11(12), p.125405.

[Mcdonald, (2000)] McDonald, K. T. (2000). Bessel beams. arXiv Preprint physics/0006046.

[McGloin and Dholakia, (2005)] McGloin, D. and Dholakia, K., 2005. Bessel beams: diffraction in a new light. Contemporary Physics, 46(1), pp.15-28.

[McLaren t al., (2012)] McLaren, M., Agnew, M., Leach, J., Roux, F.S., Padgett, M.J., Boyd, R.W. and Forbes, A., 2012. Entangled bessel-gaussian beams. Optics Express, 20(21), pp.23589-23597.

[McLaren et al., (2013)] McLaren, M., Roux, F.S. and Forbes, A., 2013, August. Modal Decomposition of Bessel-Gaussian Beams. In CIOMP-OSA Summer Session on Optical Engineering, Design and Manufacturing (p. Th1). Optical Society of America.

[McLaren, (2014)] McLaren, M., 2014. Tailoring Quantum Entanglement of Orbital Angular Momentum (Doctoral dissertation, Faculty of Physics at Stellenbosch University Department of Laser Physics, University of Stellenbosch).

[McLaren et al., (2014)] McLaren, M., Mhlanga, T., Padgett, M.J., Roux, F.S. and Forbes, A., 2014, September. Entangled Bessel beams. In SPIE Optical Engineering+ Applications (pp. 919409-919409). International Society for Optics and Photonics.

[McLaren et al., 2015] McLaren, M., Konrad, T. and Forbes, A., 2015. Measuring the non-separability of classically entangled vector vortex beams. arXiv preprint arXiv:1502.02153.

[McQueen et al., (1999)] McQueen, C.A., Arlt, J. and Dholakia, K., 1999. An experiment to study a “nondiffracting” light beam. American Journal of Physics, 67(10), pp.912-915.

[Moh, K., et al, (2007)] Moh, K.J., Yuan, X.C., Bu, J., Burge, R.E. and Gao, B.Z., 2007. Generating radial or azimuthal polarization by axial sampling of circularly polarized vortex beams. Applied optics, 46(30), pp.7544-7551.

[Molloy and Padgett, (2002)] Molloy, J.E. and Padgett, M.J., 2002. Lights, action: optical tweezers. Contemporary Physics, 43(4), pp.241-258.

[Ndagano et al., (2015)] Ndagano, B., Brüning, R., McLaren, M., Duparré, M. and Forbes, A., 2015. Fiber propagation of vector modes. Optics express, 23(13), pp.17330-17336.

[Nowack, (2012)] Nowack, R.L., 2012. A tale of two beams: an elementary overview of Gaussian beams and Bessel beams. Studia Geophysica et Geodaetica, 56(2), pp.355-372.

[Ourjoumtsev, A. et al.,(2006)] Ourjoumtsev, A., Tualle-Brouri, R., Laurat, J. and Grangier, P., 2006. Generating optical Schrödinger kittens for quantum information processing. Science, 312(5770), pp.83-86.

[Padgett et al., (2004)] Padgett, M., Courtial, J. and Allen, L., 2004. Light's orbital angular momentum. Physics Today, 57(5), pp.35-40.

[Qin, Zhiyuan, et al., (2014)] Qin, Z., Tao, R., Zhou, P., Xu, X. and Liu, Z., 2014. Propagation of partially coherent Bessel–Gaussian beams carrying optical vortices in non-Kolmogorov turbulence. Optics and Laser Technology, 56, pp.182-188.

[Poon and Liu, (2014)] Poon, T.C. and Liu, J.P., 2014. Introduction to Modern Digital Holography: With Matlab. Cambridge University Press.

[Schmidt, A., et al.,(2011)] Schmidt, O.A., Schulze, C., Flamm, D., Brüning, R., Kaiser, T., Schröter, S. and Duparré, M., 2011. Real-time determination of laser beam quality by modal decomposition. Optics express, 19(7), pp.6741-6748.

[Schulze et al., (2012)] Schulze, C., Ngcobo, S., Duparré, M. and Forbes, A., 2012. Modal decomposition without a priori scale information. Optics express, 20(25), pp.27866-27873.

[Schwarz et al., (2002)] Schwarz, U.T., Sogomonian, S. and Maier, M., 2002. Propagation dynamics of phase dislocations embedded in a Bessel light beam. Optics communications, 208(4), pp.255-262.

[Stamnes, (1986)] Stamnes, J.J., 1986. Waves in focal regions: propagation, diffraction and focusing of light, sound and water waves. CRC Press.

[Trager, (2007)] Träger, F. ed., 2007. Springer handbook of lasers and optics. Springer Science and Business Media.

[Tsai et al., (2006)] Tsai, T., McLeod, E. and Arnold, C.B., 2006, August. Generating Bessel beams with a tunable acoustic gradient index of refraction lens. In SPIE Optics+ Photonics (pp. 63261F-63261F). International Society for Optics and Photonics.

[Wang et al., (2010)] Wang, X.L., Li, Y., Chen, J., Guo, C.S., Ding, J. and Wang, H.T., 2010. A new type of vector fields with hybrid states of polarization. Optics express, 18(10), pp.10786-10795.

[Woerdemann, 2012] Woerdemann, M., 2012. Structured Light Fields: Applications in Optical Trapping, Manipulation, and Organisation. Springer Science and Business Media.

[Yao et al., (2011)] Yao, A.M. and Padgett, M.J., 2011. Orbital angular momentum: origins, behavior and applications. Advances in Optics and Photonics, 3(2), pp.161-204.

[Zhan, 2009] Zhan, Q., 2009. Cylindrical vector beams: from mathematical concepts to applications. Advances in Optics and Photonics, 1(1), pp.1-57.

[Zhu and Wang, (2014)] Zhu, L. and Wang, J., 2014. Arbitrary manipulation of spatial amplitude and phase using phase-only spatial light modulators. Scientific reports, 4.